Cureus Journal of Engineering

Open Access Original Article

# Thermo-Kinetic and Synergistic Evaluation of Catalytic Co-Pyrolysis of Coal-Sewage Sludge Using Thermogravimetric Analysis (TGA)/Derivative Thermogravimetry (DTG) Analysis

**Received** 07/01/2025
**Review began** 07/14/2025
**Review ended** 12/14/2025
**Published** 01/14/2026

© **Copyright** 2026
Rabah et al. This is an open access article distributed under the terms of the Creative Commons Attribution License CC-BY 4.0., which permits unrestricted use, distribution, and reproduction in any medium, provided the original author and source are credited.

**DOI:**
https://doi.org/10.7759/s44388-025-00011-4

Muhammad Rabah [1] , Asif H. Khoja [1, 2] , Waqar Ul Habib Khan [1] , Ali Raza [1] , Abeera A. Ansari [1] , Syed S. Daood [3]

1. U.S. Pakistan Center for Advanced Studies in Energy (USPCAS-E), National University of Sciences & Technology, Islamabad, PAK 2. Environment & Chemical Engineering, University of Cincinnati, Cincinnati, USA 3. Institute of Energy & Environmental Engineering (IEEE), University of the Punjab, Lahore, PAK

**Corresponding author:** Asif H. Khoja, engr.asifglt@gmail.com

## Abstract

This study investigates the utilization of sewage sludge (SS) and low-rank coal (C) for the purpose of energy recovery by co-pyrolysis. Pyrolysis process is performed through thermogravimetric analysis and derivative thermogravimetry. The thermo-kinetic parameters are determined by applying the Coats-Redfern technique's using F1, F1.5, D1, and S1 reaction mechanistic models. The analysis determines that (Sample E), consisting of 80% coal and 20% SS, is the most effective. It demonstrates a low activation energy ($E_a$) of around 20.5 kJ/mol and 17.7 kJ/mol for models F1 and S1, respectively. These low $E_a$ values are due to the high volatile content and inherent inorganic minerals in SS, which make the decomposition reactions easier. As the concentration of SS in the mixes increases, the $E_a$ decreases. Furthermore, the mean reactivity ($R_{m.r}$) and pyrolysis factor ($P_f$) were analyzed to further assess the thermal behavior of the fuel blends. The addition of 2% $Sr_2TiFeO_6$ catalyst loading to optimum blend, i.e. CP2 leads to a maximum weight loss of 19.2% in the primary pyrolysis zone, while $E_a$ decrease from 20.5 kJ/mol to 13.6 kJ/mol for Model F1. The study's findings highlight the promising potential of catalytic co-pyrolysis of coal-sludge for improved energy recovery.

**Categories:** Bioprocess Engineering, Catalysis and Reaction Engineering, Chemical Process Optimization
**Keywords:** catalytic co-pyrolysis, sewage sludge, coats redfern method, waste to energy, thermo-kinetics

## Introduction

Growing energy demand continues to put pressure on fossil fuel resources and contributes to higher greenhouse gas emissions. According to the International Energy Agency (IEA), global energy-related $CO_2$ emissions increased by about 6% in 2021 as economies recovered after the COVID-19 pandemic [1]. This steady rise in emissions highlights the need for cleaner and more sustainable energy options. Researchers are investigating green energy alternatives to reduce $CO_2$ emissions and limit fossil fuel consumption [2].

Coal power stations are projected to generate approximately 10,415 TWh in 2023 to around 13,317 TWh by 2040 [3]. However, coal, despite being the world’s largest energy source, still faces several challenges. Combustion of coal generates significant amounts of ash, and the development of new coal reserves often requires extensive transportation infrastructure to reach processing facilities. Additionally, the burning of low-quality coal releases greenhouse gases (GHGs). Due to these adverse effects, there is pressing need to reduce or eliminate the use of coal in the global energy industry [4].

Sewage sludge (SS) production is rising due to rapid urbanization and stricter effluent discharge rules worldwide. Approximately 80% of sludge production fails safety and stability tests [5]. Traditional disposal methods are no longer effective. SS's enormous volume and physicochemical features cause wastewater treatment plant (WWTP) operators to spend more than 30% of their operational costs on its handling. Thus, socio-economic and environmental issues support alternative SS treatment and disposal options [6].

Thermochemical methods, specially pyrolysis, change the perception of SS to be considered a resource rather than waste by converting it into products like biochar, bio-oil, and biogas [7]. However, pyrolysis of pure SS often produces low-quality and low-energy products. This highlights the need for co-pyrolysis with coal and the potential use of catalysts, such as perovskites, to improve process efficiency, addressing a critical gap in existing literature.

**How to cite this article**
Rabah M, Khoja A H, Khan W, et al. (January 14, 2026) Thermo-Kinetic and Synergistic Evaluation of Catalytic Co-Pyrolysis of Coal-Sewage Sludge Using Thermogravimetric Analysis (TGA)/Derivative Thermogravimetry (DTG) Analysis. Cureus J Eng 3 : es44388-025-00011-4. DOI https://doi.org/10.7759/s44388-025-00011-4

Co-pyrolysis of SS and other feedstocks may solve these issues by improving pyrolysis bioproduct quality and quantity [8]. Various raw materials, including microalgae, rice straw, and manure, have been employed in co-pyrolysis alongside SS [9]. The co-pyrolysis of SS and coal offers a potential reduction in GHG emissions while simultaneously producing bioenergy. The combined use of coal and SS can potentially offset their limitations. Pyrolysis and co-pyrolysis have some drawbacks. The bio-products produced are thermally unstable, and their refining into biofuels or chemicals is often more complex and, at times, more expensive [10]. Catalytic co-pyrolysis enhances calorific value, reduces bio-oil oxygen content, and improves the stability of bioproducts. Catalysts interact with pyrolysis vapors to enhance the quality or distribution of the products [11]. Earlier investigations explored zeolite and metal oxide-based catalysts, encompassing $Al_2O_3$, CaO, $Fe_2O_3$, $TiO_2$, and ZnO, for SS pyrolysis. Combining these metal oxides with active metals leads to the restructuring of volatile vapors [12]. However, challenges exist with these catalysts; zeolite-based catalysts tend to deactivate rapidly in biomass catalytic pyrolysis. Additionally, metal-based catalysts present high costs, low selectivity, susceptibility to impurity poisoning, and potential environmental harm [13]. In this study, double perovskite $Sr_2TiFeO_6$-based (STF) catalyst, with a chemical formula of A2BB′O6, AA′B2O6, or AA′BB′O6, is employed due to its adjustable catalytic activity, thermal stability, and technical viability [14]. Double perovskites are preferable to single perovskites due to their improved chemical stability in redox, acidic, essential, and high-temperature conditions. Due to its distinctive structure, perovskite oxides can be adjusted both in terms of physical and chemical properties to suit various applications in energy and environmental catalysis [15].

This study specifically focuses on exploring the suitable blending ratios and operating conditions that can be chosen for scaled-up operations in a pyrolysis reactor. Decision-making in larger-scale facilities is crucial and is based on a synergistic evaluation of blends to achieve maximum yield and reactivity with or without a catalyst. The study examines the effect of catalyst loadings and determines the kinetic parameters via Coats-Redfern methods obtained from TGA. This study will contribute to optimizing thermochemical decomposition energy by revealing the catalyst's impact on blend activation energies and decomposition zones. The acquired knowledge can then be applied to select the operating temperature based on the desired reaction rate and product outcomes. This involves sizing the reactor based on kinetics, ensuring efficient control of the process, and enabling the prediction of reaction rates.

# Materials And Methods

## Sample collection and blends preparation

SS was collected from the local WWTP. The collected SS was sun-dried for 2 days and then oven-dried at 105°C for 24 hours to remove moisture and achieve a consistent dry weight. Pure bituminous coal (C) was collected from Baluchistan, Pakistan. Samples of C and SS were both crushed with a pestle and mortar separately and later sieved at 0.2 mm using the Sieving RX-29-10, WS Tyler (USA).

*Coal-Sewage Sludge (C-SS) Blends Preparation*

Sieved pure bituminous coal (C) and SS samples were mixed thoroughly at different ratios to prepare blends. The weighted ratios of SS were 0%, 5%, 10%, 15%, and 20% (on a dry basis). Pure bituminous coal (C) and SS samples were also kept as controls. Table *1* shows the composition and sample code for prepared (C-SS) blends.

| Sample | Composition by dry wt. (%) | |
|---|---|---|
| Code | Coal (%) | Sludge (%) |
| A | 100 | 0 |
| B | 95 | 5 |
| C | 90 | 10 |
| D | 85 | 15 |
| E | 80 | 20 |
| F | 0 | 100 |

**TABLE 1: Identities and Compositions of Coal and Sewage Sludge Blends**

*Catalyst Loaded C-SS Blends*

The catalyst used in this investigation was $Sr_2TiFeO_6$-(STF), which is synthesized using the sol-gel-assisted glycine-nitrate combustion process. The chemical solution was made by dissolving metal nitrate salts in stoichiometric proportions of Sr and Fe (2:1, each) in deionized water. In contrast, titanium isopropoxide was dissolved at room temperature in ethanol. A viscous gel was formed by evaporating the mixture of the two solutions over a hot plate at a temperature of 90°C while stirring continuously. The temperature of the hot plate was then raised to 300°C, which resulted in the gel's auto-ignition and the generation of black STF ash. The self-combusting gel was then dehydrated in a preheated oven at 120°C for 12 hours overnight. After air drying, the black ash was calcined at 900°C for 3 hours to produce pure black double perovskite STF powder [16]. The selected optimal blend from C-SS blends was loaded with the given catalyst with different loading ratios by weight using a GSM weight scale. The in-situ approach was used to prepare the sample, whereby the catalyst was directly mixed with the optimal blend. After adding the given ratio of catalyst in the blend, the blends were thoroughly mixed to ensure uniform distribution of the catalyst by using a vortex mixer [17]. The composition of prepared catalytic blends is given below in Table *2*.

| Sample | Composition by dry wt. (%) | |
|---|---|---|
| Code | Blend | Catalyst (STF) |
| CP1 | 99 | 1 |
| CP2 | 98 | 2 |
| CP3 | 97 | 3 |
| CP4 | 96 | 4 |

**TABLE 2: Identities and Compositions of Catalytic Loaded Blends**

## Characterization techniques

Each sample of the prepared coal and sewage sludge (C-SS) blend weighed 80 mg and had a particle size of 0.2 mm. The CHN Analyzer (5ECHN2200, CKIC, China) was used to determine the proportion of carbon, hydrogen, and nitrogen in each sample by comparing it with the standard values. Sulfur Analyzer 5E-IRS II (CKIC, China) was used to determine the S content in (C-SS) blends. For the sulfur analyzer, a 300 mg weight sample with a 0.2 mm particle size was obtained. The ($N_2$, $O_2$, and He) gases were used to calculate the percentage. The oxygen content was measured by the difference method. However, the uncertainty associated with this approach is acknowledged. Proximate Analysis of the sample, including the moisture content, volatile matter, fixed carbon, and ash, was evaluated following the American Society of Testing Materials (ASTM) standard methods of ASTM E872-82 (2006), ASTM E1755-1 (2007), and ASTM E871-82 (2019) [18].

Gross Calorific Value (GCV) analysis was carried out following the procedure (ASTM D5865-13), using the PAR-6200 bomb calorimeter to determine the gross calorific values of the prepared (C-SS) blend samples. Fourier Transform Infrared Spectroscopy (FTIR) analysis was conducted to identify the various functional groups and chemical bonds present in the (C-SS) blend samples. A Cary 630 FTIR (Agilent Technologies, USA) with a diamond ATR module was employed to analyze the samples in the 500-4000 $cm^{-1}$ wavelength range.

## Co-pyrolysis in TGA

TGA and DTG were performed on a TGA 5500 (TA Instruments, USA). The prepared (C-SS) blend samples were heated from room temperature to 900°C in a nitrogen ($N_2$) atmosphere. The nitrogen flow rate was maintained at 25 $mL.min^{-1}$, while the co-pyrolysis was carried out at a heating rate of 20°C $min^{-1}$.

*Synergistic Effect*

The synergistic effect was found by comparing the blend's calculated and experimental values. The additive model assumed no coal-biomass interactions during co-pyrolysis and produced (Equation 1) [19].

$$Y_{\text{cal}} = X_{\text{SS}} \cdot Y_{\text{SS}} + X_{\text{coal}} \cdot Y_{\text{coal}} \quad (1)$$

Here, the calculated value is donated as $Y_{cal}$. $Y_{coal}$ and $Y_{ss}$ represent the experimental values of coal and SS, respectively, while $X_{coal}$ and $X_{SS}$ represent the mass ratios of coal and SS in the (C-SS) blends. When generating theoretically described thermal decomposition parameters for TGA and DTG curves, all

samples were considered. To understand the co-pyrolysis interactions, the residue left must be considered. Equation (2) investigated and quantified the synergistic and anti-synergistic interactions based on experimental and computed data differences [20].

$$\text{Deviation} = \left(\frac{\text{Exp}_{\text{value}} - \text{Cal}_{\text{value}}}{\text{Cal}_{\text{value}}}\right) \times 100\% \quad (2)$$

## Model-fitting thermo-kinetic study

The Coats-Redfern method was used to determine the kinetic characteristics of prepared (C-SS) blends. Kinetics parameters were calculated using the Arrhenius law, which supplies information regarding the reaction rate. The fundamental equation utilized for the kinetic study of (C-SS) blends co-pyrolysis is given in (Equation 3) [21].

$$\frac{d\alpha}{dt} = k(T)f(\alpha) \quad (3)$$

Where dα/dt is the reaction rate change, f(α) is the reaction model, and k(T) is the rate constant. α is the conversion factor representing weight loss, as shown in Equation (4).

$$\alpha = \frac{w_i - w_t}{w_i - w_f} \quad (4)$$

Here "$w_i$" indicates the initial weight of the sample, "$w_t$" is the weight at the given or instantaneous time, and $w_f$ is the final weight after the completion of the process. Furthermore, k(T) can be calculated using Equation (5).

$$k(T) = A \cdot \exp\left(\frac{-E_a}{RT}\right) \quad (5)$$

Where A is an pre-exponential factor taken in ($s^{-1}$), R is the universal gas constant having the value of (R = 0.008314 $kJ.K^{-1}.mol^{-1}$), T is the absolute temperature in kelvin (K), and the $E_a$ represents the activation energy (kJ/mol). By substituting the value of k(T) in Equation (5) to Equation (3), we can get Equation (6):

$$\frac{d\alpha}{dt} = A \cdot \exp\left(\frac{-E_a}{RT}\right) \cdot f(\alpha) \quad (6)$$

It is well-known that TGA experiments have a constant heating rate ( $\beta$), which is defined as $\beta = \frac{dT}{dt}$. By putting it in Equation (6), we get the resulting Equation (7) as follows:

$$\frac{d\alpha}{dT} = \frac{A}{\beta} \cdot \exp\left(\frac{-E_a}{RT}\right) \cdot f(\alpha) \quad (7)$$

If we apply integration to Equation (7), then it becomes as follows:

$$g(\alpha) = \int^{\alpha} \frac{d\alpha}{\quad} = \frac{A}{\quad} \int^{T} \exp\left(\frac{-E_a}{\quad}\right) \quad (8)$$

In Equation (8), g(α) is the reaction model integral form. The right side of the equation is difficult to solve; hence, different approximation models were utilized. The kinetic properties of (C-SS) blends and catalyst-loaded optimum (C-SS) blends were assessed using the Coats-Redfern method. The Coats-Redfern method used the integral function g(α) to estimate the solid breakdown rate. When utilizing the Coats-Redfern approach, it is necessary to ascertain its apparent $E_a$ and the reaction order. Finally, the reaction order was used to express the final form, equivalent to unity in this investigation. Therefore, Equation (9) became as follows:

$$\ln\left(\frac{g(\alpha)}{T^2}\right) = \ln\left(\frac{AR}{\beta E_a}\left(1 - \frac{2RT}{E_a}\right)\right) - \frac{E_a}{RT} \quad (9)$$

Where $\left(1-\frac{2RT}{E_a}\right)$ is assumed to be small and can be neglected from Equation (9). Hence, it can be written as presented in Equation (10), also for a first-order reaction g(α) = -ln (1-α):

$$\ln\left(\frac{g(\alpha)}{T^2}\right)=\ln\left(\frac{AR}{\beta E_a}\right)-\frac{E_a}{RT} \quad (10)$$

From graph between $\ln[g(\alpha)/T^2]$ vs 1/T, $E_a$ was obtained using the slope of the line and "A" was obtained using the same graph's intercept, which gives a straight line.
All non-catalytic and catalytic C-SS blends were subjected to reaction models listed in Table 3 using available literature [22]. Using earlier studies, models were chosen based on their more significant linear regression (R2) and most suitable kinetic and thermodynamic parameters. The present study utilized previously documented models [23] about the Parabolic law (D1), chemical reaction order (F1, F1.5), and the geometrical column of phase interfacial reaction shrinkage (S1).

| Model | f(α) | g(α) |
|---|---|---|
| F1 | 1st order (n = 1) | $-\ln(1-\alpha)$ |
| F1.5 | 1 and half order (n = 3/2) | $2\left[(1-\alpha)^{-\frac{1}{2}}-1\right]$ |
| D1 | Parabolic law | $\alpha^2$ |
| S1 | Shrinkage Geometric Column | $1-(1-\alpha)^{1.5}$ |

**TABLE 3: Reaction Mechanisms and Models for Kinetic Study**

### Reactivity analysis

Relative mean reactivity ($R_{m.r}$) and pyrolysis factor ($P_f$) were calculated using TGA and DTG data for sample A, Sample F and their blend. $R_{m.r}$ quantifies the reactivity of the material and is expressed as Equation (11), which is the ratio of the maximum decomposition rate to the corresponding peak temperature [8,24,25]:

$$R_{\mathrm{m.r}}=\frac{\mathrm{DTG_{max}}}{T_{\mathrm{pk}}} \quad (11)$$

where $DTG_{max}$ (wt.%/°C) is the maximum rate of mass loss, and $T_{pk}$ (°C) is the peak degradation temperature.

To further assess the pyrolysis efficiency, the pyrolysis factor ($P_f$) was calculated [26,27], as shown in Equation (12):

$$P_{\mathrm{f}}=\frac{\mathrm{DTG_{max}}\times\mathrm{DTG_{avg}}}{T_{\mathrm{st}}^2\times T_{\mathrm{fn}}} \quad (12)$$

Where, $DTG_{avg}$ is the average degradation rate (wt.%/°C), $T_{st}$ and $T_{fn}$ are initial and final pyrolysis temperature. This factor integrates thermal reactivity and volatilization characteristics, offering a comprehensive measure of pyrolysis performance [8,27,28].

### Catalytic co-pyrolysis in TGA

Catalytic co-pyrolysis of the optimum blend over the catalyst was performed on a TGA 5500 (TA Instruments, USA). The samples were loaded into a platinum crucible pan and heated from 25°C to 900°C in an inert atmosphere at a constant heating rate of 20°C/min with a nitrogen flow rate of 25 $mL.min^{-1}$. The weight of the sample loaded was 10 mg. Before experimenting, each sample was purged at $N_2$ for 30 minutes.

## Results And Discussion

### Physiochemical behavior of C-SS blends

Table 4 represents the ultimate analysis (CHNS-O) of (Coal/C/Sample A) and (Sewage Sludge/SS/Sample F). The analysis showed that the carbon, hydrogen, nitrogen, and sulfur content of (Sample A) were 68.08%, 3.85%, 1.28%, and 0.48%, respectively. The ultimate analysis is in accordance with the literature [17]. The oxygen content was calculated by the difference method, which is 26.31%. The carbon, hydrogen, nitrogen, and sulfur contents of (Sample F) were 27.70%, 5.85%, 4.20%, and 0.32%, respectively. The presence of oxygen content in (Sample F) was 61.93%, calculated by difference. The presence of oxygen content in (Sample F) was more than that in (Sample A) and is related to the amount of moisture that is present in it. A higher content of hydrogen indicates that (Sample F) is suitable as an alternative and as a secondary fuel for (sample A) in co-pyrolysis. The H/C atomic ratio evaluates the energy content of any fuel, the higher the H/C ratio the lesser will be the oxidation reactions thus releasing much energy content [29] and providing more hydrogen resources to play a dominant role in hydrogenation [30]. The H/C atomic ratio of (Sample A) was (0.674) which is far less than (2.517) for (Sample F). GCV describes a material's energy content and is the most crucial metric to determine sample combustibility. The GCV of (sample F) was 13.43 MJ/kg, and of (Sample A) was 28.5 MJ/kg.

According to the proximate analysis, the biomass mainly comprised volatile matter, which holds promise for conversion into bioenergy products. Furthermore, the lower ash content may signify a greater yield of bio-oil. The quality of biomass products is significantly affected as the ash content in biomass rises. In (Sample A), the moisture content was found to be 2.10%, volatile matter was 29.30% while the fixed carbon was 55.70% and ash was 12.90%, while for (sample F) the moisture content was found to be 22%, which is in accordance with the oxygen content described in the ultimate analysis, volatile matter was 53% while the fixed carbon was 9.40% and ash was 15.6% as shown in Table 4.

| Sample code | Coal (A) | Sewage Sludge (F) |
|---|---|---|
| Ultimate Analysis | | |
| Carbon (C%) | 68.08 | 27.7 |
| Hydrogen (H%) | 3.85 | 5.85 |
| Nitrogen (N%) | 1.28 | 4.2 |
| Sulfur (S%) | 0.48 | 0.32 |
| Oxygen[a] (O%) | 26.31 | 61.93 |
| H/C | 0.674 | 2.517 |
| GCV (MJ/kg) | 28.5 | 13.43 |
| Proximate analysis | | |
| Moisture content | 2.1 | 22 |
| Volatile matter | 29.3 | 53 |
| Fixed carbon | 55.7 | 9.4 |
| Ash content | 12.9 | 15.6 |

**TABLE 4: Ultimate and Proximate Analysis of Coal and Sewage Sludge**

[a]: By difference

C-SS blends FTIR spectra are given in Figure 1. (Sample A) has a shallow peak at 3340 $cm^{-1}$ in the 3000-3800 $cm^{-1}$ wavelength range. Single bond -OH stretching vibration causes this low peak intensity. A high peak at 3642 $cm^{-1}$, indicating crystal water in the clay minerals [31], and another strong peak at 2896 $cm^{-1}$ caused by aliphatic C-H groups stretching vibration [32] were observed in (Sample A). The shallow C=C peaks in the range of 1500-2200 $cm^{-1}$ were mostly aliphatic and aromatic [33]. A resonance at 1590 $cm^{-1}$ suggests aromatic nucleus C=C stretching vibration, which indicates the abundance of carbon in (Sample A). Peaks were present in the range of 1000-1500 $cm^{-1}$ band, which can be attributed to alcohols, phenols, carbonyls, and carboxyl [34]. Asymmetric deformation vibration of $CH_2$ and $CH_3$ may create another peak at 1416 $cm^{-1}$. The Si-O-Si symmetric stretching link caused the coal spectra to peak at 1039 $cm^{-1}$ [35]. The comparatively weak zone was observed at 700-900 $cm^{-1}$, which is induced due to the out-of-plane bending of aromatic C-H groups [36].

FTIR spectra of (Sample F) shown in Figure 1 show H-bonded and N-H groups in the spectral region of

3100-3600 $cm^{-1}$ [37]. (Sample F) has a more substantial broad stretching peak, which is attributed to the -OH group stretching vibration occurring in the range of 3100-3600 $cm^{-1}$ indicating that (Sample F) had more -OH groups (free water) than (Sample A). O-H stretching of carboxylic and alcoholic groups caused a prominent peak at 3262 $cm^{-1}$. A broad peak attributed to aliphatic C-H stretching was observed in the range of 2800-3000 $cm^{-1}$. COOH's C-H and -OH stretching causes the 2940 $cm^{-1}$ peak. This wavelength's functional group is -CH, which presumably produces CH4. (Sample F) lipids decompose into alkanes, chiefly CH4 [38]. No sharp peaks were observed for aromatic nucleus C=C stretching vibration which shows lower carbon content in (Sample F) as compared to (Sample A). Aliphatic C-H deformation caused the second significant absorbent peak at 1418 $cm^{-1}$. Primary alcohol C-O-H stretching causes a peak at 1010 $cm^{-1}$ [39]. The stretching of alcohol and carbohydrates caused 1000-1100 $cm^{-1}$ peaks, indicating the presence of polysaccharides, especially cellulose, a critical organic component of (Sample F).

Compared to (Sample A), (C-SS) blends had higher absorbance intensity at 900-1200 $cm^{-1}$. (Sample B) had the highest absorption intensity in this range of all (C-SS) blends. (C-SS) blends had lower absorbance intensities as (Sample F) content increased. (Sample B), (Sample C), (Sample D), and (Sample E) have respective peaks at 1037 $cm^{-1}$, 1032 $cm^{-1}$, 1030 $cm^{-1}$, and 1029 $cm^{-1}$. As the content of (Sample F) in (C-SS) blends rises, there is a decrease in the intensity of absorbance peaks. This spectral region exhibits peaks attributed to C=C bending and alcohols. A notable peak at 3640 $cm^{-1}$ observed in all (C-SS) blends indicates the presence of the -OH group [40]. The (coal/Sample A) sample exhibited this distinctive peak, and with an increase in sludge content, the absorption intensity peaks in this region decreased for the blends.

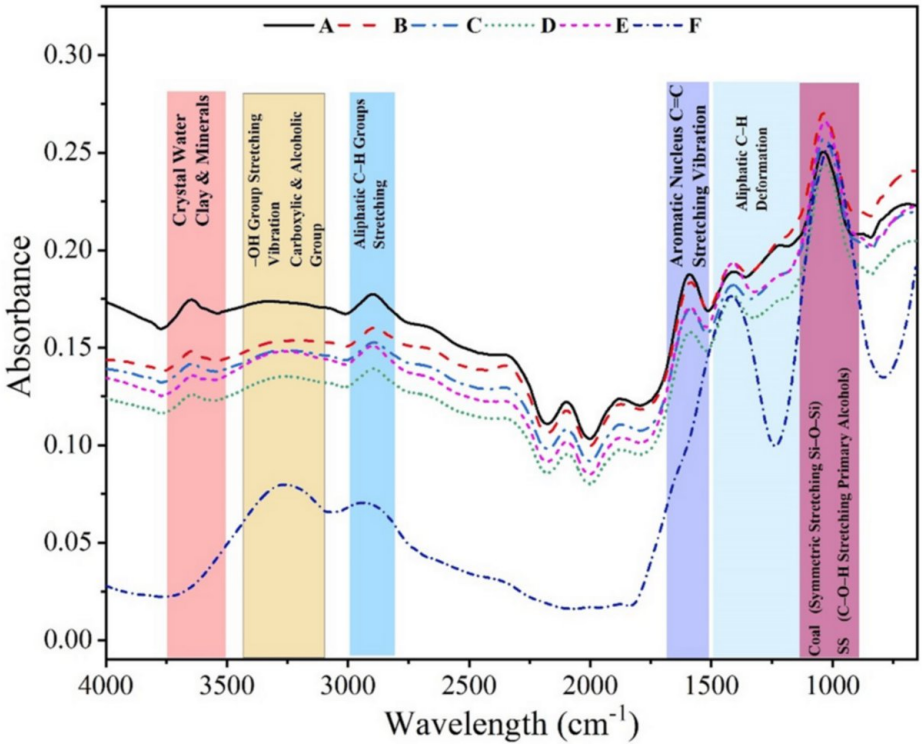



**FIGURE 1: FTIR Spectra of C-SS Blends**

FTIR, Fourier Transform Infrared; C-SS, coal and sewage sludge

## Catalyst properties

The physiochemical properties of the employed catalyst are shown in Figure *2*(A,B,C,D). X-ray diffraction (XRD) spectra were obtained to study the synthesized STF catalyst's crystal structure insights, as shown in Figure *2A*. The synthesized STF was observed to have a double perovskite structure with a cubic structure in the pm-3m space group. The surface morphology of the catalyst was studied using SEM. As shown in Figure *2B*, STF possesses a porous, web-like morphology. To verify the porous structure of the catalyst, N2 physisorption was performed, as shown in Figure *2C*. STF was found to possess a surface area of 45.78 $m^2/g$. The thermal stability of the catalyst was studied using TGA as shown in Figure *2D*; the catalyst was highly stable, as no significant weight loss occurred even at 900°C. The excellent thermal stability and surface reactivity of STF make it a feasible catalyst for multiple thermo-catalytic applications [16].

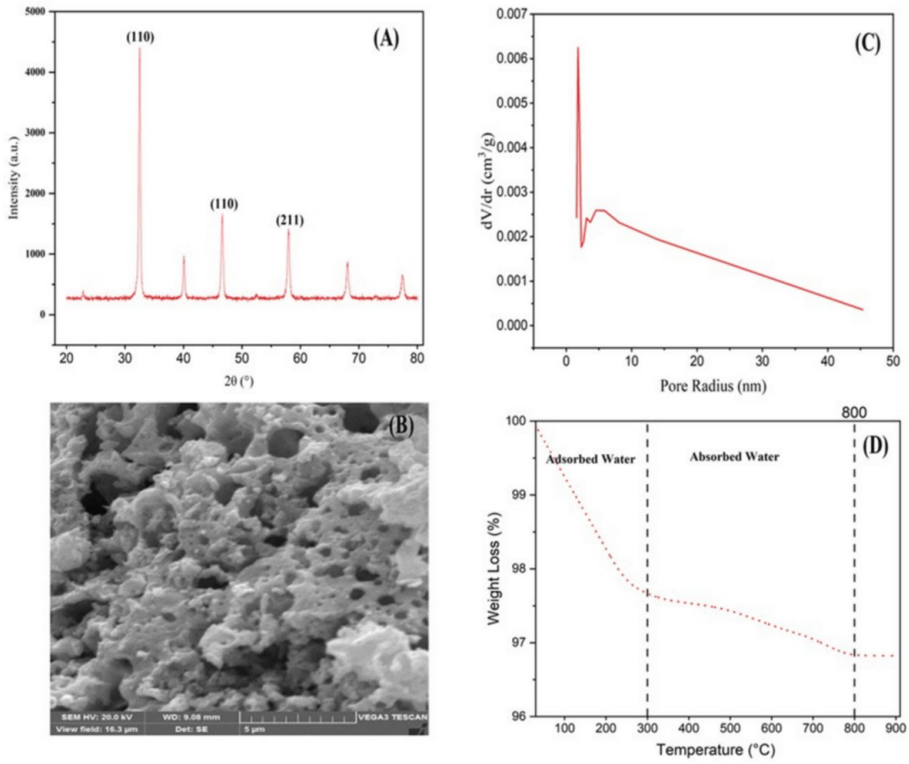



**FIGURE 2: Catalyst Characterizations (A) XRD Spectra of STF, (B) SEM Image of STF at 10 µm, (C) BJH Pore Size Distribution, (D) TGA of STF**

XRD, X-ray diffraction; SEM, Scanning Electron Microscopy; TGA, Thermogravimetric Analysis

## Co-pyrolysis of C-SS blends in TGA

Figure *3*(a-b) and Figure *4*(a-b) shows TGA and DTG analysis of (C-SS) blends, respectively. Dotted and solid lines show TGA and DTG profiles versus reaction temperature. Table *5* illustrates three sites for (C-SS) blends TGA and DTG curves. The TGA and DTG curves of (C-SS) blends are divided into three stages: moisture, low-temperature volatiles, high-temperature volatiles, and char. These elements affect weight loss (ML%) and combustion in these areas [41]. The residue left (RL%) represents the solid residue after thermal decomposition in the TGA, reflecting the non-volatile fraction remaining at the end of the heating process.

(Sample A) lost 3.2% weight at 25-180°C in the first stage which is moisture loss, as seen in Figure *3*(a). The DTG curve indicates that a peak was achieved at 161.1°C in the first stage as shown in Figure *4*(a). Following the removal of surface water, depolymerization took place in the second stage region-III, where the DTG curve peaked at 460°C and most of the volatiles were removed at that point, possibly due to carbon-containing volatile materials [42] as shown in Figure *3*(a). The TGA curve showed that (coal/Sample A) lost 22% of its weight between 400 and 650°C, which is an active pyrolysis zone where most of the devolatilization occurs. In the third stage, almost 5% of the weight loss occurred in the temperature range of 650-900°C due to the slow decomposition of the char produced, and no significant peaks were observed in this stage as shown in Figure *4*(a). An overall 32.71% ML for (coal/Sample A) was observed from the TGA profile as shown in Figure *3*(a).

Figure *3*(a) shows a (Sewage Sludge/Sample F) TGA curve; in the first stage at 25-180°C, a loss of 4.7% weight occurs in which the dehydration of organic compounds was observed. As in Figure *4*(a), in the parent samples, DTG a curve with a modest peak at 74.2°C was observed for (Sample F). When light volatile compounds are released, (Sewage Sludge's) chemical structure depolymerizes and softens [43]. The most ML% in (Sample F) occurred within the temperature range of 180-650°C, which is the second stage and consists of two regions. The TGA curve shows that almost 46% of weight loss occurred in both regions of this stage as shown in Figure *3*(a). Here the DTG curve exhibited two peaks. A moderate peak was observed at 289°C in Region-II, and another peak was observed at 531°C in Region-III within the specified temperature range, as shown in Figure *4*(a). Reactive organic components in the material begin to decompose at this stage, which is why it is called an "active pyrolysis stage" [44]. For (Sewage Sludge/Sample F), the third stage or region-IV occurs in the temperature range of 650-900°C and comprises the breakdown of (Sewage Sludge), which concludes between 655 and 740°C as shown in Figure *3*(a), with the DTG curve reaching its peak at 706 °C. Within this range, almost 8% of the weight loss occurred as shown in Figure *4*(a). The breakdown involves inorganic compounds such as calcium

carbonate and microcline, contributing to this weight loss. The sluggish decomposition of inorganic compounds, such as carbonaceous waste and non-biodegradable materials in this zone, is the cause of this phenomenon [45]. An overall 58.43% ML for (sewage sludge/Sample F) was observed from the TGA profile as shown in Figure *3*(a).

The TGA-DTG profile of (C-SS) blends was similar to those of their constituent materials, although their intensities and sharpness varied depending on coal and SS proportions as shown in Figure *3*(b) and Figure *4*(b). In the first stage which occurs within the temperature range of 25-180°C, all four blends showed a slight rise between 40 and 130°C due to higher moisture present in the blends due to SS, which leads to a weight loss of 2-3.5% in this region as shown in Figure *4*(b). The peak in this region became more distinct with an increased concentration of SS and lies in the peak temperature range of 53-64°C. The second stage in (Sample B) comprises two regions, i.e. region-II and region-III which occur within the temperature range of 180-650°C. In region-II 3% weight loss occurred which is attributed to its low SS concentration as shown by the TGA curve in Figure *3*(b) no prominent peak was observed in this region, while in the second stage region-III a prominent DTG peak was observed with a peak temperature of 472 °C due to presence of coal and its breakdown as shown in Figure *3*(b). In this region, 23% of weight loss is observed in the TGA profile shown in Figure *3*(b). In the third stage and region-IV which occurs within the temperature range of 650-900°C, a prominent peak was observed at 692°C in the DTG profile, and in this stage, almost 21.56% weight reduction occurred. An overall 50.28% ML for (Sample B) was observed from the TGA profile as shown in Figure *3*(b). The TGA and DTG curves of (Sample C) displayed a 4.05% weight loss in the second stage region-II having a peak temperature of 305°C mostly associated with the devolatilization of SS in the blend at an earlier temperature while in second stage region-III weight loss of 18% is observed. A sharp peak was also observed in this region having a peak temperature of 462.5°C where devolatilization occurs due to the presence of constituents of coal in the blend at a delayed temperature. In the third stage, region-IV weight loss of about 14% occurs due to the slow decomposition of the char produced after devolatilization, a prominent peak was observed having a peak temperature of 699°C as shown in Figure *3*(b) and Figure *4*(b). An overall ML% of 38.04% has been observed in (Sample C). (Sample D) and (Sample E) TGA and DTG curves are illustrated in Figure *3*(b) and Figure *4*(b). In the second stage, region-II of (Sample D) and (Sample E) DTG curves, 5% and 6.5% weight loss, respectively, was observed having peak temperatures of 315°C and 317°C showing the decomposition of volatiles present in the blends at lower temperature. A second peak was observed in the second stage region-III where (Sample D) and (Sample E) have 16% and 19% weight loss due to the decomposition of coal which explains the second temperature range in the DTG curves for blends. In this temperature range, SS decomposition was low having peak temperatures of 461.9°C and 465.6°C. In the third stage, region-IV of (Sample D) and (Sample E) 9.5% and 16% of weight loss occurred due to its coal content getting lower and SS concentration getting higher and predominant peaks were observed for both blends having peak temperatures of 688 °C and 703 °C which depicts the slow decomposition of the char as shown in Figure *3*(b) and Figure *4*(b). An overall ML% of 33.29% and 44.79% has been observed in (Sample D) and (Sample E). As the SS concentration in the blend increases, weight loss fluctuates within the parent sample range.

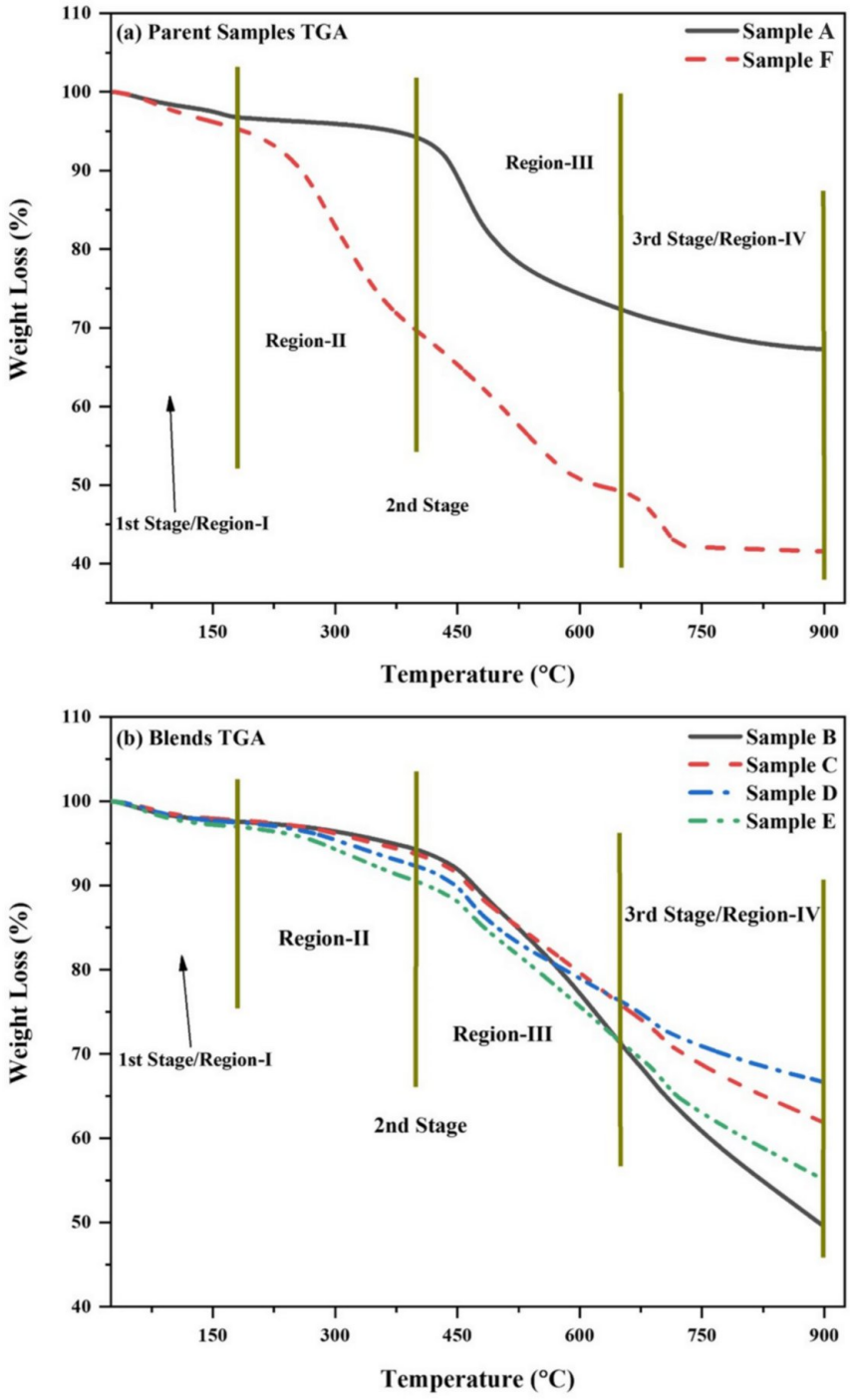



**FIGURE 3: TGA profile of C-SS blends (a) TGA of Parent Samples (b) TGA of Blends**

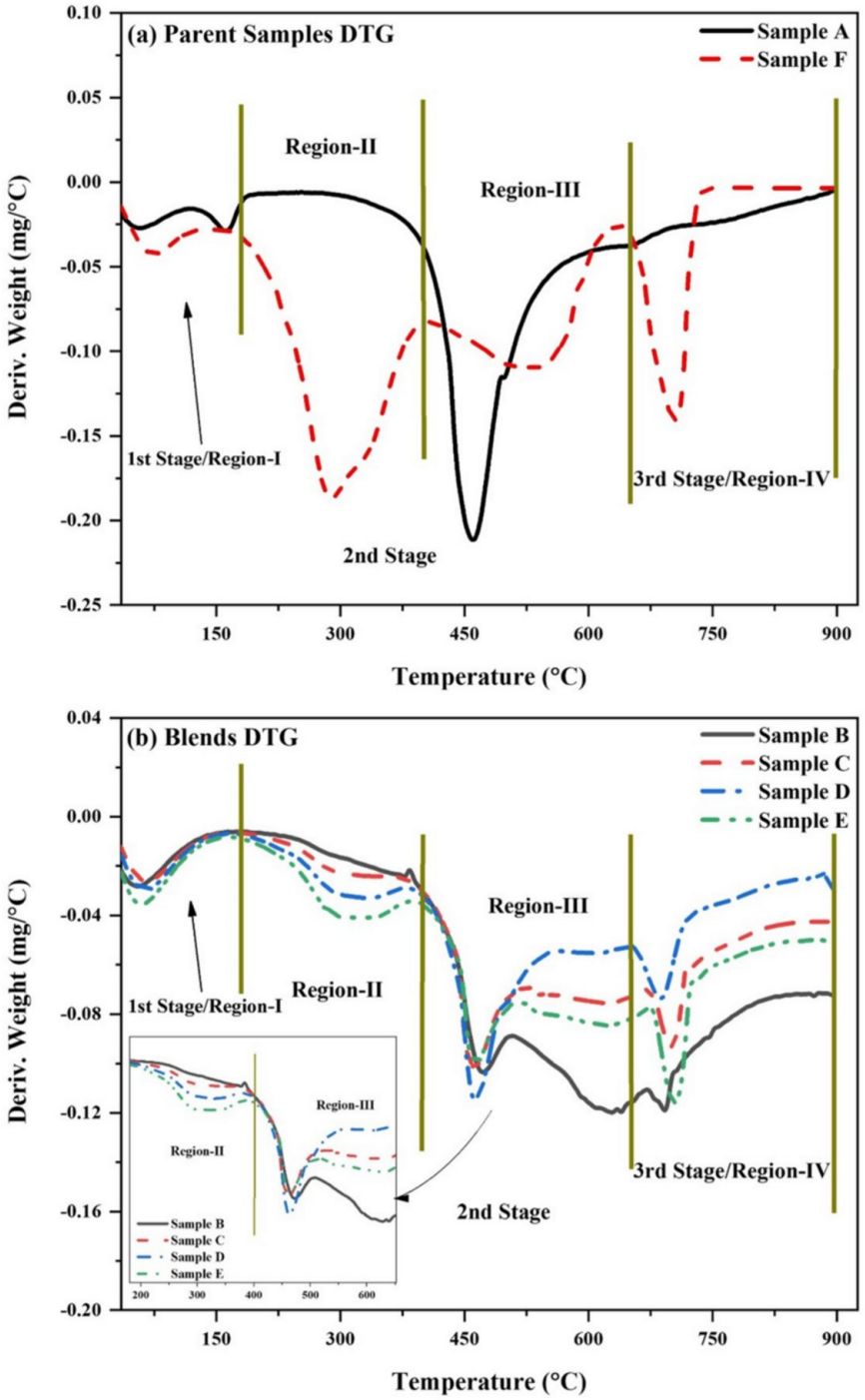



**FIGURE 4: DTG Profile of C-SS Blends (a) DTG of Parent Samples (b) DTG of Blends**

DTG, derivative thermogravimetry; C-SS, coal and sewage sludge

| Sample code | 1st Stage/Region-I (25-180°C) | | | | 2nd Stage (180-650°C) | | | | | | | | 3rd Stage (650-900°C) | | | |
|---|---|---|---|---|---|---|---|---|---|---|---|---|---|---|---|---|
| | | | | | Region-II (180-400°C) | | | | Region-II (400-650°C) | | | | | | | |
| | $T_{pk}$ | ML% | RL% | DTG (wt.%/°C) | $T_{pk}$ | ML% | RL% | DTG (wt.%/°C) | $T_{pk}$ | ML% | RL% | DTG (wt.%/°C) | $T_{pk}$ | ML% | RL% | DTG (wt.%/°C) |
| A | 161.1 | 3.23 | 96.77 | -0.02876 | - | 2.57 | 94.2 | - | 460 | 21.83 | 72.37 | -0.21136 | - | 5.08 | 67.29 | - |
| B | 53.04 | 2.423 | 97.577 | -0.02814 | - | 3.338 | 94.239 | - | 472 | 22.957 | 71.2822 | -0.10359 | 692 | 21.5622 | 49.72 | -0.11896 |
| C | 63.91 | 2.261 | 97.739 | -0.02613 | 305 | 4.045 | 93.694 | -0.03202 | 462.5 | 17.8 | 75.894 | -0.10249 | 699 | 13.94 | 61.959 | -0.09323 |
| D | 60.71 | 2.518 | 97.482 | -0.02974 | 315 | 5.202 | 92.28 | -0.03231 | 461.9 | 16.009 | 76.2709 | -0.1147 | 688 | 9.5569 | 66.714 | -0.07351 |
| E | 59.03 | 3.0407 | 96.959 | -0.03534 | 317 | 6.493 | 90.466 | -0.04088 | 465.6 | 19.015 | 71.4514 | -0.09925 | 703 | 16.24 | 55.211 | -0.11577 |
| F | 74.2 | 4.6918 | 95.3082 | -0.04253 | 289 | 25.67 | 69.638 | -0.18653 | 531 | 20.41 | 49.2285 | -0.1103 | 706 | 7.6594 | 41.569 | -0.14059 |

**TABLE 5: TGA-DTG Profile Parameters of (C-SS) Blends**

$T_{pk}$: Peak degradation temperature, ML%: Mass loss percentage, RL%: Residue left percentage, DTG: Maximum derivative thermogravimetry.
TGA, thermogravimetric analysis; C-SS, coal and sewage sludge

*Synergistic Effect of C-SS Blends in Co-Pyrolysis*

Experimental and calculated weight loss and residual fraction results were compared to understand prepared blend synergy. Table *6* shows the experimental-calculated weight loss difference. (Sample D) projected weight loss (36.56%) exceeded its actual weight loss (33.28%), suggesting a negative synergistic effect [46]. However, (Sample D) exhibited an overall positive synergistic effect concerning the residue left.

In comparison, (Samples B, C, and E) showed greater values for experimental weight loss than calculated weight loss, indicating an overall positive synergistic effect. In terms of deviation, (Sample B) revealed the highest deviation (47.88%), followed by (18.22%) of (Sample E) and (7.82%) of (Sample C). Increasing SS content in blends showed a decreasing deviation trend from (Sample B) to (Sample D), but (Sample E) exhibited an increase in the deviation, which could be attributed to higher than the needed concentration of SS in the blend. Weight loss in (C-SS) blends is associated with the degradation of organic and volatile compounds in SS fraction. Heavy metals and inorganic matter in sewage sludge also give rise to a catalytic effect and enhanced biomass conversion, resulting in increased beneficial synergistic impact in weight loss among (C-SS) blends [30]. Thus, a blend with a higher biomass ratio is selected as an optimum blend i.e. (Sample E) for bio-oil generation.

| Blend | Blend ID | Experimental ML % | Calculated ML% | Deviation |
|---|---|---|---|---|
| 95Coal:5SS | B | 50.28 | 34 | 0.479 |
| 90Coal:10SS | C | 38.04 | 35.28 | 0.078 |
| 85Coal:15SS | D | 33.28 | 36.56 | -0.089 |
| 80Coal:20SS | E | 44.75 | 37.85 | 0.182 |

**TABLE 6: Synergistic Effect of C-SS Blends Co-Pyrolysis**

C-SS, coal and sewage sludge

*Model-Fitting Thermo-Kinetic Study of (C-SS) Blends*

Kinetic data are essential for co-pyrolysis energy production since $E_a$ represents activation energy and 'A' represents collision frequency. $E_a$ is calculated from the slope of the Arrhenius law, whereas the intercept helps estimate A [47]. The kinetic parameters of (C-SS) blends are shown in Table *7*. Coal and SS DTG profiles vary depending on their organic and inorganic content and "rank." Sludge's organic component is not coalified. Organic matter breakdown causes coal's high-temperature peak. Sludge has two lower-temperature peaks than coal. At lower temperatures, minimal complex organic structures degrade; at

higher temperatures, complex structures decompose and devolatilize [48]. Based on the DTG peak regions, the decomposition process was divided into three distinct temperature ranges: the 1st decomposition region (150-400°C), the second decomposition region or primary pyrolysis region (400-650°C), and the third decomposition region or high-temperature region (650-900°C).

The initial decomposition range peak was SS-dominated. In this range, coal decomposes slowly. As SS concentration grew, blend Ea increased. Biomass volatiles generate carbonaceous deposits on coal particles, slowing reactions and raising $E_a$ [49]. Models F1, D1, and S1 show the same increasing $E_a$ trend. F1 and S1 showed the lowest $E_a$ for the (C-SS) blends. The models also exhibited the lowest linear regression for blends, which is the most essential factor. D1 consistently had the highest linear regression for all blends in this range of the model. The best linearity for the initial temperature range was found using first-order and one-dimensional models utilizing the Coats-Redfern integral technique.
All DTG curves demonstrated that coal in blends caused the degradation peak in this range. The ease of (C-SS) blends decreased as SS increased. All samples had high linear regression in all models. However, model S1 had the lowest $E_a$ for SS and blends. F1 and S1 model's $E_a$ values were much higher than their first-range values. These findings suggest that primary biomass decomposition may degrade tarry compounds. Charring also increases activation energy by producing carbon [50]. Model D1 has a negative $E_a$ value because of SS's complicated composition and its involvement in complex reaction mechanisms [51].
The blend DTG peak in this range is attributed to inorganic materials and carbonates in SS. (Sample E) had the highest $E_a$, while (Sample F) had the lowest. In this range, blends have higher $E_a$ than parent fuel samples. Pore structures in the residual materials may have increased apparent $E_a$ values across all models at these temperatures, although such samples usually require higher temperatures.
The optimal blend was chosen for catalytic studies based on kinetics and synergistic effects to investigate how catalyst activity affects $E_a$, thermal decomposition ranges, and co-pyrolysis product distribution. Overall (Sample B) exhibited higher $E_a$ and weight loss than (Sample E) in a co-pyrolysis zone. (Sample E) outperformed (Sample B) in kinetic and thermodynamic experiments. (Sample B) had 34 kJ/mol Ea, while (Sample E) had 17 kJ/mol.

| Models | Blend | 1st Decomposition range | | | 2nd Decomposition range | | | 3rd Decomposition range | | |
|---|---|---|---|---|---|---|---|---|---|---|
| | | 150-400°C | | | 400-650°C | | | 650-900°C | | |
| | | Ea (kJ/mol) | A ($sec^{-1}$) | $R^2$ | Ea (kJ/mol) | A ($sec^{-1}$) | $R^2$ | Ea (kJ/mol) | A ($sec^{-1}$) | $R^2$ |
| F1 | A | - | - | - | 42.09 | 86.26 | 0.941 | - | - | - |
| | B | 1.27 | 0.001 | 0.354 | 36.9 | 13.78 | 0.997 | 31.89 | 4.846 | 0.999 |
| | C | 3.57 | 0.006 | 0.766 | 24.71 | 1.902 | 0.948 | 33.36 | 6.979 | 0.996 |
| | D | 5.83 | 0.021 | 0.856 | 26.24 | 3.601 | 0.978 | 27.87 | 3.63 | 0.993 |
| | E | 6.01 | 0.022 | 0.863 | 20.53 | 0.912 | 0.984 | 32.46 | 6.591 | 0.993 |
| | F | 20.88 | 4.022 | 0.985 | 0.993 | 0.007 | 0.112 | 7.4 | 543.208 | 0.935 |
| (F1.5) | A | - | - | - | 51.15 | 542.665 | 0.959 | - | - | - |
| | B | 1.44 | 0.001 | 0.4 | 39.63 | 24.172 | 0.997 | 45.65 | 50.792 | 0.999 |
| | C | 3.86 | 0.007 | 0.779 | 27.23 | 3.422 | 0.946 | 51.12 | 135.609 | 0.995 |
| | D | 6.32 | 0.027 | 0.86 | 31.22 | 10.879 | 0.984 | 47.25 | 104.695 | 0.995 |
| | E | 0 | 0 | 0.901 | 0 | 0 | 0.713 | 0 | 0 | 0.181 |
| | F | 23.02 | 7.71 | 0.984 | 1.37 | 0.036 | 0.357 | 0 | 0 | 0.488 |
| (D1) | A | - | - | - | 67.15 | 2218.373 | 0.915 | - | - | - |
| | B | 10.85 | 0.004 | 0.9 | 75.82 | 2681.139 | 0.998 | 37.93 | 4.891 | 0.999 |
| | C | 14.89 | 0.025 | 0.933 | 51.96 | 75.874 | 0.968 | 32.23 | 2.531 | 0.998 |
| | D | 18.72 | 0.132 | 0.943 | 47.54 | 58.511 | 0.976 | 20.49 | 0.426 | 0.977 |
| | E | 19.21 | 0.13 | 0.944 | 42.31 | 16.29 | 0.991 | 33.68 | 2.982 | 0.996 |
| | F | 43.04 | 198.102 | 0.988 | -3.92 | -0.005 | 0.734 | 12.68 | 0.138 | 0.896 |
| (S1) | A | - | - | - | 39.19 | 22.048 | 0.946 | - | - | - |
| | B | 1.07 | 0 | 0.294 | 34.27 | 2.637 | 0.997 | 20.36 | 0.281 | 0.999 |
| | C | 3.28 | 0.002 | 0.752 | 22.31 | 0.533 | 0.949 | 19.05 | 0.247 | 0.996 |
| | D | 5.05 | 0.008 | 0.823 | 21.67 | 0.632 | 0.969 | 12.95 | 0.091 | 0.978 |
| | E | 5.09 | 0.007 | 0.808 | 17.68 | 0.227 | 0.984 | 20.64 | 0.327 | 0.993 |
| | F | 18.86 | 1.08 | 0.984 | -5.18 | -0.005 | 0.88 | 22.09 | 0.664 | 0.926 |

**TABLE 7: Kinetic Parameters of (C-SS) Blends**

$E_a$: Activation energy, A: Pre-exponential factor, $R^2$: Regression factor. C-SS, coal and sewage sludge

## Reactivity analysis

The reactivity of coal, sludge, and their blend was analyzed using $R_{m.r}$ and $P_f$, following Ghetti et al. [52]. According to the value of $R_{m.r}$ presented in Table *8*, sewage sludge shows the highest reactivity, followed by coal and then the blend. The total mass loss (ML%) was 32.7% for Sample A, 58.43% for Sample F, and 44.79% for Sample E, corresponding to $R_{m.r}$ values of $0.4595 \times 10^{-3}$, $0.6454 \times 10^{-3}$, and $0.2132 \times 10^{-3}$, respectively. The Pyrolysis Factor ($P_f$), which integrates devolatilization rate and pyrolysis temperature to assess pyrolytic behavior, followed a similar trend as reactivity analysis. This confirms the higher thermal degradation behavior of sewage sludge, likely due to its higher volatile content and faster decomposition kinetics compared to coal. The calculated $P_f$ values are also depicted in Table *8*, which reinforce the conclusion that sewage sludge possesses enhanced reactivity and performance.

| Sample | $T_{st}$ (°C) | $T_{pk}$ (°C) | $T_f$ (°C) | $DTG_{max}$ (wt.%/°C) | $DTG_{avg}$ (wt.%/°C) | $R_{m.r}$ ($10^{-3}$ wt.%/min.°C) | $P_f$ ($10^{-8}$) |
|---|---|---|---|---|---|---|---|
| A | 400 | 460 | 650 | -0.21136 | -1.74808 | 0.4595 | 0.3553 |
| E | 400 | 465.6 | 505 | -0.09925 | -1.40352 | 0.2132 | 0.1699 |
| F | 180 | 289 | 400 | -0.18653 | -2.33282 | 0.6454 | 3.3578 |

**TABLE 8: Reactivity Analysis Parameters of (C-SS) blends**

$T_{st}$: Starting pyrolysis temperature, $T_{pk}$: Peak degradation temperature, $T_f$: Final pyrolysis temperature, $DTG_{max}$: Maximum derivative thermogravimetry, $DTG_{avg}$: Average derivative thermogravimetry, $R_{m.r}$: Mean reactivity factor, $P_f$: Pyrolysis factor. C-SS, coal and sewage sludge

## Catalytic co-pyrolysis of C-SS blends

*FTIR Analysis of Catalytic C-SS Blends*

Figure 5 shows the FTIR spectra of four catalyst-loaded optimum blend. In the range of 3000-3600 $cm^{-1}$, a noticeable and broad peak was observed. The blends CP1, CP2, CP3, and CP4 had respective peaks at 3421 $cm^{-1}$, 3419 $cm^{-1}$, 3431 $cm^{-1}$, and 3431 $cm^{-1}$, which occurred due to the presence of H- and N-H bonds in this region. Two peaks were noticed for all-catalytic samples in the 2800-3000 $cm^{-1}$ region. The existence of aliphatic C-H stretching vibration is primarily responsible for these peaks, and the functional group corresponding to this wavelength is -CH. It is mostly due to the breakdown of lipids into alkanes in SS [53]. A strong peak was found between 1640-1520 $cm^{-1}$. Aromatic C═C stretching in the coal and SS are the primary functional groups responsible for this increase in peak. At 1441 $cm^{-1}$, 1433 $cm^{-1}$, 1441 $cm^{-1}$, and 1436 $cm^{-1}$, a moderate peak was seen for CP1, CP2, CP3, and CP4. Aliphatic C-H deformation, the benzene ring, and the methoxy group in the biomass are the primary causes of absorption peaks in this region [54]. A broad peak was observed in the range of 900-1100 $cm^{-1}$ for all catalytic blends, which- is due to the C-O stretching vibration. This indicates that the macromolecular structure of biomass contained abundant alcoholic hydroxyl groups, phenolic hydroxyl groups, and ether bonds. The minor peaks and shoulders in the FTIR spectra of the blends coalesce between 650-900 $cm^{-1}$ range. When compared to CP1, CP2, and CP3, CP4 displayed the highest absorbance peaks. Peaks in this region are mostly caused by polycyclic, single, and substituted aromatic groups [55]. All blends significantly peaked at 540 $cm^{-1}$, suggesting $TiO_2$ stretching [56]. This peak was hardly existent in CP1 but grew larger in CP2, CP3, and CP4, with the latter showing the sharpest peak. Peak sharpness is proportional to the amount of catalyst present in the blends. A shallow peak was observed in blends CP1, CP2, and CP3 at 459 $cm^{-1}$,461 $cm^{-1}$, and 466 $cm^{-1}$, respectively, corresponding to Si-O-Si or O-Si-O bending modes [57].

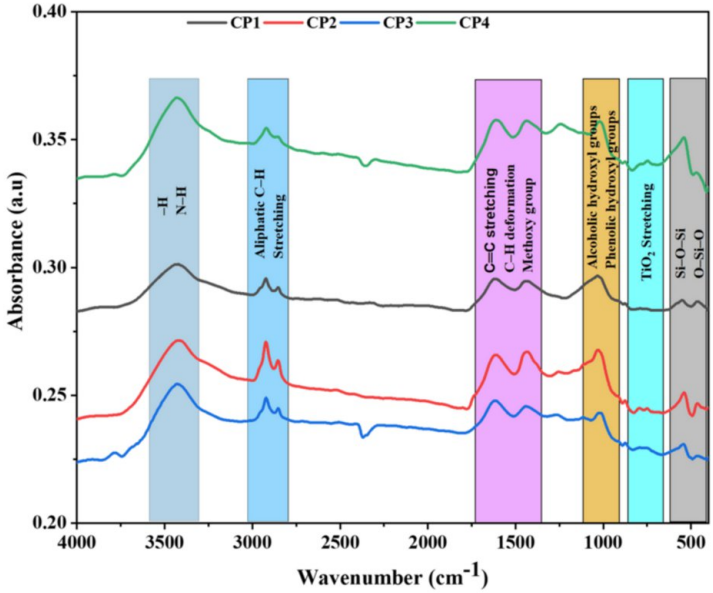



**FIGURE 5: FTIR Spectra of Catalyst Loaded C-SS Blends**

FTIR, Fourier Transform Infrared; C-SS, coal and sewage sludge

*TGA and DTG Analysis of Catalytic C-SS Blends*

Figure 6 and Table 9 show catalytic blend TGA and DTG curves. All catalytic blends had TGA curves similar to Sample E (optimal non-catalytic blend) with sharper peaks. TGA curves indicated that blends lose less weight as catalyst concentration increases. Stability and char generation improved with catalysts. Due to higher weight loss, the non-catalytic blend was better for bio-oil generation.

Figure 6(a-b) shows TGA and DTG curves of catalyst blends, respectively. The TGA curve showed a CP1 sample weight loss of about 35%. The TGA curve of CP1 showed about 22% weight loss in both regions of the second temperature range (180-650°C). The third decomposition range lost 10.4% weight. CP2 TGA curve shows a 42.41% weight loss, the highest among all blends in Figure 6(a). Sample CP2 lost weight (25.4%) in both regions of the second temperature range (180-650°C). The third decomposition range (650-900°C) saw 14.9% weight loss. Sample CP3's TGA curve in Figure 6(a) indicated over 40% weight reduction. The TGA curves of CP3 showed 24% weight loss in the 180-650°C range and 14% in the 650-900°C range. CP4's TGA curve in Figure 6(a) exhibited the lowest weight reduction of all mixes, 32%. TGA curves of CP4 showed a 22% weight loss in the 180-650°C temperature range but only 8% in the third temperature range. The in-situ addition of a catalyst to the sample increases residue as the catalyst concentration increases.

Bio-products and weight loss were caused by SS organic matter devolatilization. High temperatures aided this process by breaking strong organic bonds and releasing energy. Increasing pyrolysis temperature boosted bio-oil extraction yields, reaching 460°C. All catalytic blends had substantial peaks between 450 and 470°C, with CP4 having the highest peak. Catalyst loading decreased weight loss in the third decomposition range. The DTG curve showed a high at roughly 700°C in this location. CP2 had the region's highest peak, followed by CP3's peak. CP4 had the shallowest peak. The decline in weight loss in the third temperature range (650-900°C) was likely due to secondary reactions, such as the thermal cracking of volatile chemicals, an endothermic reaction that becomes significant at temperatures above 500-550°C [58]. TGA study showed that catalytic co-pyrolysis of C-SS to create bio-oil was best with 2% STF catalyst loading since CP2 had the most significant weight loss, and the second temperature range was optimal.

CP4, with the lowest weight loss, was the best choice for catalytic co-pyrolysis of C-SS blends to make biochar. The third decomposition range was best for char production since the char produced remained consistent with only a slight decline. Catalysts also lower the temperature range's temperature peaks. As the catalyst concentration increased, temperature peaks dropped. CP2 peaked at 720°C, CP3 at 703°C. CP1 peaked at 695°C. CP4, an ideal char-producing catalytic blend, peaked at 692°C. The non-catalytic optimal blend peak was 703°C. It reveals that the catalyst helps attain the maximum peak at a lower temperature due to its activity in char-forming processes [59].

| Blend | Range 1 | | | | Range 2 | | | | Range 3 | | | |
|---|---|---|---|---|---|---|---|---|---|---|---|---|
| | 150-400 (°C) | | | | 400-600 (°C) | | | | 650-900 (°C) | | | |
| | $T_p$ (°C) | ML (%) | RL (%) | DTG (%/°C) | $T_p$ (°C) | ML (%) | RL (%) | DTG (%/°C) | $T_p$ (°C) | ML (%) | RL (%) | DTG (%/°C) |
| CP1 | 316 | 6.8 | 91.1 | -0.04 | 463 | 13.2 | 77.9 | -0.1 | 695 | 6 | 69.1 | -0.08 |
| CP2 | 317 | 6.3 | 91.7 | -0.03 | 466 | 15.1 | 76.6 | -0.09 | 720 | 8.1 | 64.3 | -0.1 |
| CP3 | 308 | 6.6 | 91.3 | -0.03 | 462 | 14.1 | 77.2 | -0.09 | 703 | 7.4 | 65.8 | -0.1 |
| CP4 | 332 | 6.7 | 91.5 | -0.04 | 462 | 13.3 | 77.7 | -0.11 | 692 | 5 | 70.8 | -0.06 |

**TABLE 9: Catalytic Co-Pyrolysis Parameters of C-SS Blends**

C-SS, coal and sewage sludge

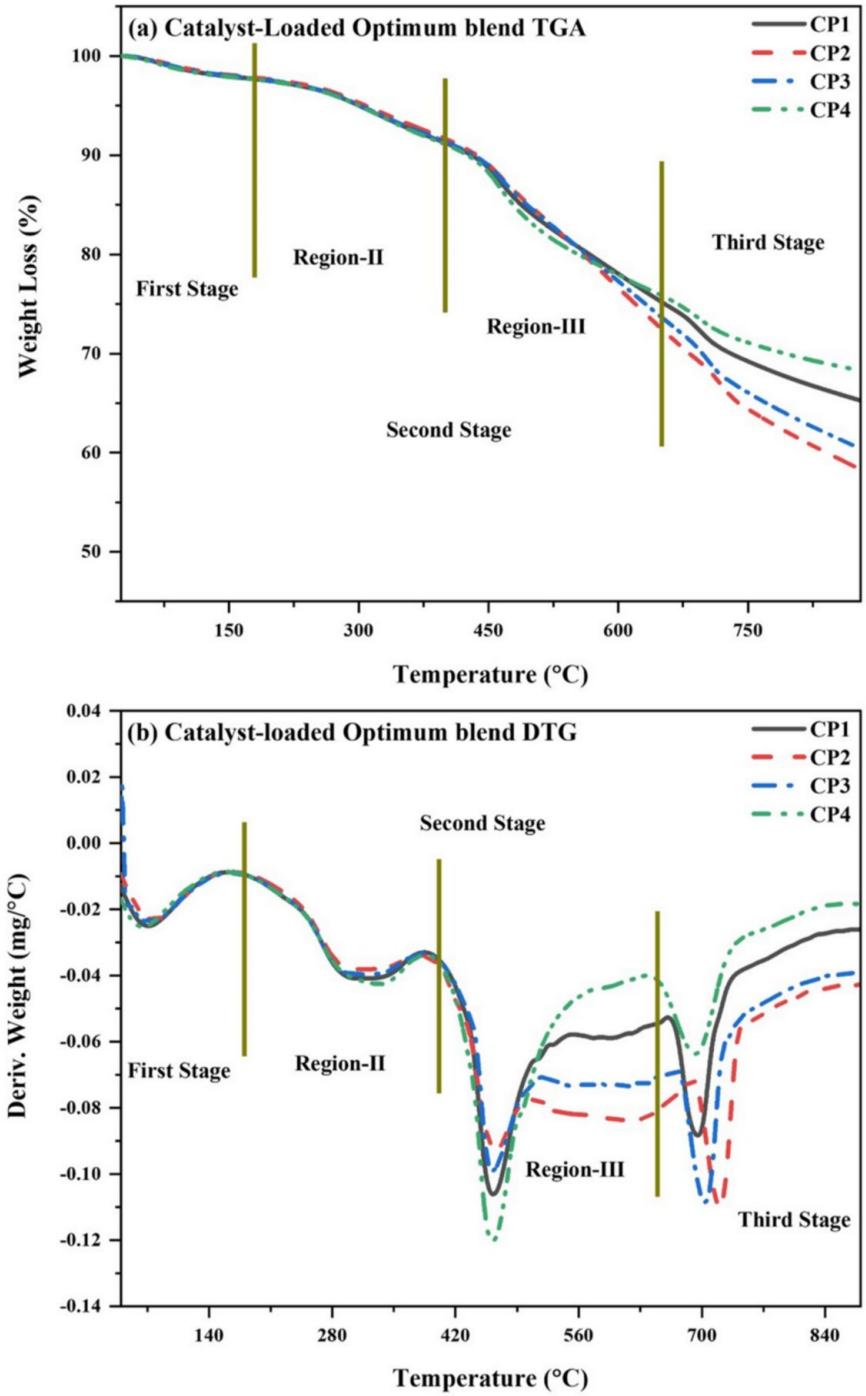



**FIGURE 6: TGA-DTG Profile of Catalyst-Loaded Optimum Blend (a) TGA (b) DTG**

TGA, thermogravimetric analysis; DTG, derivative thermogravimetry

*Model-Fitting Thermo-Kinetic Study of Catalyst-Loaded Optimum Blend*

This study used four kinetic models for kinetic analysis. This study selected optimal kinetic models for co-pyrolysis based on their performance in determining the ideal blending ratio, which is critical for achieving an efficient and sustainable pyrolysis process. For catalytic pyrolysis, the selection of the best kinetic models was dictated by their capability to identify the optimum catalyst loading ratio, thereby maximizing the yield and quality of the end products. The sample was catalyzed to improve the co-pyrolysis reaction's secondary reaction. A catalyst reduced Ea significantly compared to co-pyrolysis without a catalyst. Kinetic analysis was performed at Stage II, the primary pyrolysis zone. Kinetic analysis

began at 180-400°C. This range isn't the central pyrolysis zone; catalytic activity has little effect on Ea. The lowest Ea value was found in CP2. The D1 model indicated few Ea values as unfavorable, possibly due to the complex reaction mechanisms explained in the last section. Models F1 and F1.5 had improved kinetic characteristics in the specified temperature range. Second stage kinetic parameters are higher than the first stage. According to the Arrhenius equation, the collision frequency in each zone is proportional to the activation energy [60].

The active pyrolytic zone, or second decomposition zone (400-650°C), showed catalytic activity. All kinetic models showed a decrease in catalytic sample Ea values. Table *10* shows that model F1, (Sample E) has an Ea value of 20.5 kJ/mol, while the catalytic samples have a lower value. Ea values for CP2 and CP3 were 13.6 and 13 kJ/mol, respectively, while CP2 had a higher linear regression, indicating better kinetic properties. The CP2 and CP3 had the lowest Ea values for model F1.5. The CP2 was the best fit for model F1.5 because it performed better in linear regression despite a slight variation in Ea. Model D1 had a linear regression of 0.97 with Ea values of 42 kJ/mol for (Sample E) and 32 kJ/mol for CP2. Model S1 had the highest linear regression and lowest Ea for CP2. Ea dropped in the first region and rose in the second due to the cessation of catalytic co-pyrolysis, which produced small molecules by secondary cracking of intermediate compounds [61]. Table *10* shows the catalyst's influence in the second decomposition zone. The catalyst decreased the blend Ea significantly. This decline may be attributable to the presence of Fe in the STF. Another study found that the catalyst's effect on the C-C and C-H cleavage makes the Ea go down when Fe metal is added to the catalyst [62]. This decline in Ea can also be attributed to the larger surface area that STF possesses. Thus, it is more beneficial for the distribution of active sites of STF, which speeds up the decomposition of SS pyrolytic volatiles in the decomposition zone [63]. Additionally, when an activating agent is used, more initially reactive molecules transform into activated molecules. Thus, the Ea falls as reactant molecules per unit volume increase [64]. According to observations, the F1 and S1 models had the best overall performance in the second decomposition zone. Additionally, the sample CP2 had the highest values of linear regression and the lowest values of Ea in this range for models F1 and S1. Therefore, we can also postulate CP2 as the best-performing sample in the second decomposition range.

The third decomposition range is due to SS's inorganic and metal content. As seen in section 3.4.3, TGA analysis showed modest weight loss in this range. Ea dropped significantly in this temperature range, from 32 kJ/mol for blend E to 17 kJ/mol in the CP2.

Time and temperature increase the overall difference between Ea, which may impede the conversion process. Section 3.4.2 TGA analysis shows that sample weight loss decreases between the second and third decomposition ranges. Compared to non-catalytic samples, catalytic samples had higher energies but lower Ea values. In conclusion, the catalyst affected degradation rates and reduced the energy needed for the co-pyrolysis of blends [65].

| Models | Blend | 1st Decomposition range | | | 2nd Decomposition range | | | 3rd Decomposition range | | |
|---|---|---|---|---|---|---|---|---|---|---|
| | | 150-400°C | | | 400-650°C | | | 650-900°C | | |
| | | Ea (kJ/mol) | A ($sec^{-1}$) | $R^2$ | Ea (kJ/mol) | A ($sec^{-1}$) | $R^2$ | Ea (kJ/mol) | A ($sec^{-1}$) | $R^2$ |
| (F1) | Blend E | 6.018 | 0.022 | 0.863 | 20.53 | 0.912 | 0.984 | 32.465 | 6.591 | 0.993 |
| | CP1 | 10.25 | 0.099 | 0.976 | 22.87 | 1.909 | 0.973 | 17.55 | 0.632 | 0.921 |
| | CP2 | 9.8 | 0.066 | 0.975 | 13.6 | 0.191 | 0.935 | 17.28 | 0.694 | 0.994 |
| | CP3 | 10.13 | 0.15 | 0.978 | 13.01 | 0.179 | 0.919 | 16.3 | 0.655 | 0.989 |
| | CP4 | 10.53 | 0.156 | 0.974 | 16.59 | 0.667 | 0.906 | 15.79 | 0.509 | 0.994 |
| | Blend E | 0 | 0 | 0.901 | 0 | 0 | 0.713 | 0 | 0 | 0.181 |
| (F1.5) | CP1 | 11 | 0.13 | 0.975 | 26.89 | 4.866 | 0.973 | 27.44 | 5.174 | 0.938 |
| | CP2 | 10.37 | 0.082 | 0.975 | 15.34 | 0.312 | 0.932 | 21.88 | 0.002 | 0.984 |
| | CP3 | 10.77 | 0.159 | 0.978 | 14.87 | 0.306 | 0.917 | 21.01 | 2.295 | 0.982 |
| | CP4 | 11.38 | 0.168 | 0.974 | 19.69 | 2.15 | 0.901 | 21.85 | 2.434 | 0.985 |
| | Blend E | 19.216 | 0.13 | 0.944 | 42.31 | 16.29 | 0.991 | 33.688 | 2.982 | 0.996 |
| (D1) | CP1 | -26.83 | 0 | 0.683 | 43.6 | 30.898 | 0.983 | 20.48 | 0.413 | 0.997 |
| | CP2 | -27.26 | 0 | 0.688 | 32.17 | 2.263 | 0.971 | -12.18 | -0.001 | 0.27 |
| | CP3 | -26.96 | 0 | 0.682 | -22.46 | 0 | 0.819 | -12.57 | -0.001 | 0.299 |
| | CP4 | -26.75 | 0 | 0.681 | -21.97 | 0 | 0.798 | -13.57 | -0.001 | 0.369 |
| | Blend E | 5.092 | 0.007 | 0.808 | 17.688 | 0.227 | 0.984 | 20.644 | 0.327 | 0.993 |
| (S1) | CP1 | 9.59 | 0.039 | 0.973 | 19.15 | 0.39 | 0.972 | 9.28 | 0.041 | 0.974 |
| | CP2 | -23.47 | 0 | 0.835 | 11.21 | 0.059 | 0.938 | 13.17 | 0.084 | 0.997 |
| | CP3 | 9.6 | 0.033 | 0.976 | 11.96 | 0.052 | 0.922 | 12.14 | 0.179 | 0.997 |
| | CP4 | 9.75 | 0.053 | 0.972 | 13.67 | 0.202 | 0.912 | 10.67 | 0.158 | 0.999 |

**TABLE 10: Kinetic Parameters of Catalyst-Loaded Optimum Blend**

$E_a$: Activation energy, A: Pre-exponential factor, $R^2$: Regression factor

Table *11* shows a comparison of Ea reported in the literature for the pyrolysis and co-pyrolysis of sewage sludge, coal, and their blends. The Ea values show wide variation (20 to 280 kJ/mol), reflecting differences in feedstock composition, catalysts, and kinetic modelling approaches. Notably, the present study reports comparatively lower Ea values for Coal/SS and STF as the catalyst, indicating enhanced reactivity and catalytic effects relative to previous studies.

| Feedstock | Catalyst | Parameters | Kinetic Model | Ea (kJ/mol) | Ref. |
|---|---|---|---|---|---|
| Sewage sludge | | H.R*: 5, 10, 15 and 20°C/min | CR* method | 20.47-33.43 | [66] |
| MSS* | | H.R: 5, 10, 20 and 30°C/min; T: 25-1000°C | FWO method | 107.17 | [67] |
| | 30%-cata* | | | 56.47 | |
| RS* | | HR: 10 and 40°C/min | DAEM | 189.5 | [68] |
| | RM* | | | 169.4 | |
| | $Fe_2O_3$ | | | 175.4 | |
| Baiyinhua (BYH) coal | | HR: 10–50°C/min; T: 30°C to 900°C | Model-free methods | 282.7 | [69] |
| | $Fe_2O_3$ | | | 179.29 | |
| | RM* | | | 222.44 | |
| Bituminous Coal | | HR: 20°C/min; T: 25-900°C | CR method | 39 | [70] |
| Coal/SS | | HR: 20°C/min; T: 25-900°C | CR method | 20.5 | This study |
| | STF | | | 13.6 | |

**TABLE 11: Comparison of Activation Energies and Kinetic Models Reported in Previous Pyrolysis Studies**

MSS*: Municipal sewage sludge, RS*: Raw sludge, RM*: Red mud, BYH*:Baiyinhua, H.R*: Heating rate, CR*: Coats-redfern

*Possible/Approximate Reaction Mechanism*

Perovskites, known for their affordability and high catalytic activity, have been widely studied [71]. Their distinct structure offers exceptional tunability in their chemical compositions, allowing a range of physiochemical properties suitable for multiple energy and environmental catalytic applications. They exhibit enhanced chemical stability in acidic, essential, and high-temperature environments, making them efficient alternatives to noble metal catalysts [15]. Their unique ABO3-type crystal structure, thermochemical durability, and low cost make them ideal for high-temperature catalysis, including biomass pyrolysis, reforming, and product synthesis [72]. This section discusses the effect of the catalyst on the product distribution, energy recovery, and chemical composition of (C-SS) blends during catalytic co-pyrolysis, as shown in Figure 7.

The TGA of catalytic blends revealed the influence of Iron (Fe), Titanium (Ti), and Strontium (Sr) oxides present in the STF on the product distribution of catalytic co-pyrolysis. With increasing catalyst concentration, the TGA analysis of catalytic blends revealed increased biochar generation. In the two regions of the second temperature range (180-650°C), the weight loss curves of catalytic blends exhibited roughly the same pattern as the non-catalytic blend, with a slight increase in weight loss. In the third decomposition zone (650-900°C), catalytic and non-catalytic blends displayed different TGA curves. CP4 and (Sample E) lost 22% and 26% weight in the two regions of the second decomposition zones, respectively. In the third decomposition zone (650-900°C), CP4 only lost 8% of its weight, whereas (Sample E) lost 16%. Fe may contribute to weight loss reduction in the third temperature range. Adding Fe to catalytic blends slows the breakdown of organic materials, leading to more biochar. Fe in STF may improve SS decomposition in blends at first and second temperature ranges but impede cellulose and lignin decomposition at third temperatures. At low temperatures, Fe acted as a catalyst to speed up the cracking of volatiles into small molecules. At high temperatures, Fe speeds up aromatization reactions, which leads to the formation of large molecules (solid char) [73]. Increased weight loss in the initial decomposition zone is owing to the presence of Ti oxide in the catalyst, which stimulates the decomposition of organic matter and boosts reaction rates; as a result, the first and second temperature ranges exhibited substantial weight loss. According to Shao et al., metal oxides exhibit considerable catalytic activity in low-temperature zones but have negligible effects on the pyrolysis behavior of sewage sludge in high-temperature zones [12]. The increase in char production with the rise of catalyst loading in blends can be due to Strontium (Sr.) presence in STF, which encourages polycondensation reactions in pyrolysis intermediates [74]. STF porous morphology is also appropriate for catalyzing the reaction by providing increased surface area and decreasing weight loss as it takes in some co-pyrolysis intermediates. Coke formation on the catalyst's surface is another thing that increases the solid product yields. This was seen for all catalytic blends. On metal-based catalysts, there are typically two forms of carbon deposits.

Amorphous or layered carbon starts to oxidize around 500°C, and it's thought that filamentous carbon starts to oxidize around 600°C [75,76].

A notable drop in Ea was seen in catalytic blends for the second and third temperature ranges. This decline may be attributable to Fe in the STF, which promotes C-C and C-H cleavage and reduces Ea [62]. Thermodynamic analysis of catalytic blends shows that the ΔH values for the second decomposition zone were higher than those for the third. This tendency may result from increased char production events such as condensation and polymerization due to catalytic activity [77,78].

FTIR analysis of catalytic blends showed that aliphatic compounds increase with catalyst loading. There was also a decrease in oxygenated and nitrogen compounds in catalytic blends. The reduction in N and O compounds can be due to Ti in the STF, which can substitute N and O in compounds [79]. Catalyst encourages breaking C-C and C-O bonds, aromatic rings, and oxygen-functional groups with N compounds to make volatiles [80]. An increase in aliphatic compounds was also observed for catalytic blends. The catalytic activity may cause the cleavage of phenolics -O-$CH_3$, which are then changed into monocyclic aromatic hydrocarbons after the hydroxyl group is broken. Another possible route for increased aliphatic compounds is the cracking of long-chain fatty acids, amides, or amines present in SS due to catalytic activity into aliphatic compounds or aliphatic hydrocarbons. These aliphatic hydrocarbons can be turned into aromatic hydrocarbons through cyclization and aromatization reactions [81].

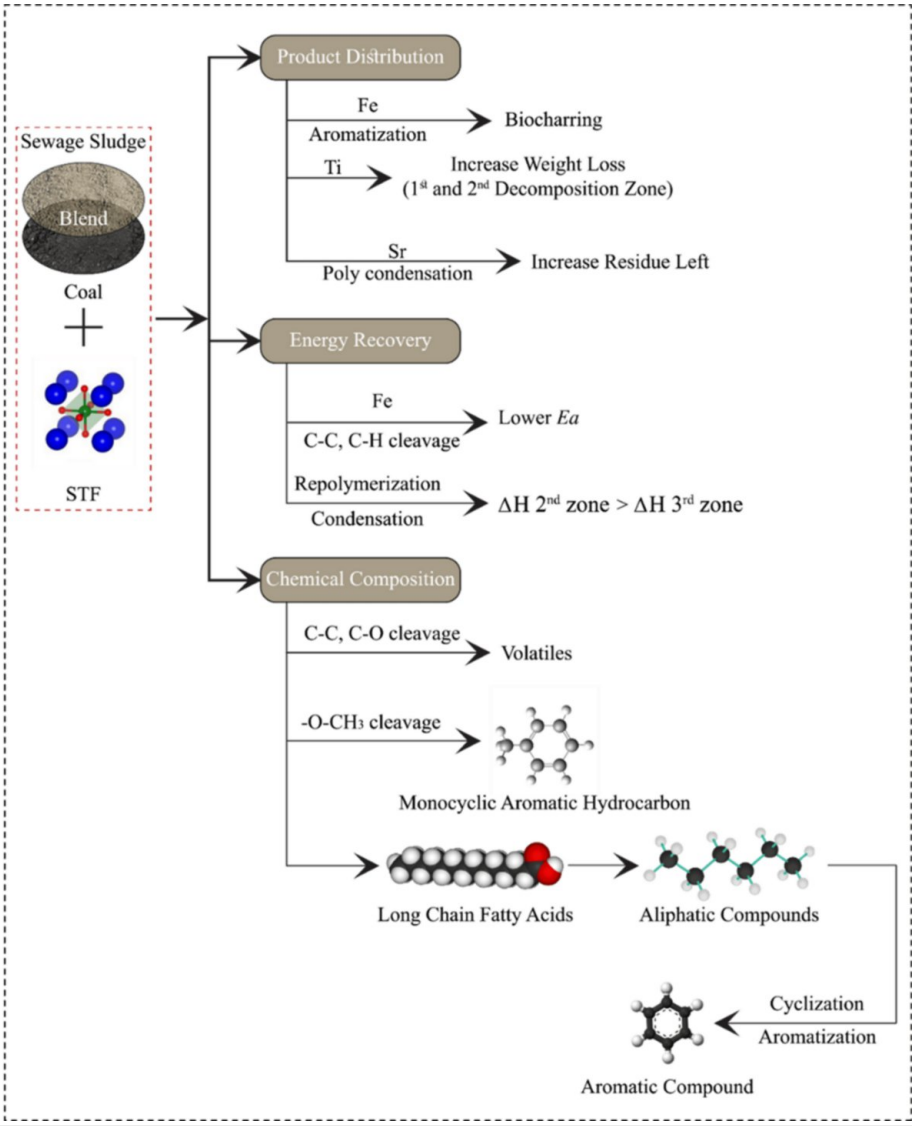



**FIGURE 7: Possible Reaction Mechanism of Catalytic Co-Pyrolysis**

## Conclusions

It is best to mix low-grade coal and sewage sludge to achieve the best results regarding carbon footprint

reduction and environmental sustainability. Coal and SS were co-pyrolyzed in a range of blending ratios. TGA and physiochemical characterizations were used to examine blends. Sample E (80C:20SS) shows optimal results among all blends regarding synergistic and kinetic parameters.

The key findings and implications of our research can be summarized as follows:

• The primary pyrolysis zone showed that (Sample E) had the lowest activation energy ($E_a$) among all (C-SS) blends, with models F1 and S1 exhibiting the most significant linear regression for (Sample E). Additionally, it was observed that Ea decreased with an increase in SS concentration in blends during the second decomposition range, and high positive synergistic effects were shown by Sample B and Sample E of (C-SS) blends.

• The performance analysis in terms of Rm and Pf showed that (Sample F/100SS) and (Sample A/100C) were more reactive than (Sample E/80C:20SS) which has the lowest performance values.

• (Sample E) was selected for further catalytic analysis to evaluate the impact of catalyst activity on $E_a$, thermal decomposition ranges, and co-pyrolysis product distribution. The catalyst $Sr_2TiFeO_6$ (STF) was loaded onto (Sample E) in different ratios.

• TGA analysis of catalytic samples indicated that an increase in catalyst concentration led to a higher residue left, while DTG peaks shifted toward char-forming catalyst activity. The study suggested that a 2% catalyst loading CP2 and its second temperature range are optimal for bio-oil production. For biochar production, 4% catalyst loading CP4 and its third temperature range is optimal, as char is produced steadily with a minor drop in this range.

• In the primary pyrolysis zone, $E_a$ was reduced, and Models F1 and S1 performed the best. Catalytic activity halved the $E_a$ in the third decomposition zone.

• The catalyst also reduced temperature peaks to lower temperatures with an increase in concentration. To advance the development of environmentally friendly procedures, further research is required which will contribute to the designing of a commercially viable catalytic co-pyrolysis reactor system, also sustainability and cost-benefit analyses are needed to make it more feasible.

# Additional Information

## Author Contributions

All authors have reviewed the final version to be published and agreed to be accountable for all aspects of the work.

**Concept and design:** Asif H. Khoja, Muhammad Rabah, Waqar Ul Habib Khan, Abeera A. Ansari, Syed S. Daood, Ali Raza

**Critical review of the manuscript for important intellectual content:** Asif H. Khoja, Waqar Ul Habib Khan, Abeera A. Ansari, Syed S. Daood, Ali Raza

**Supervision:** Asif H. Khoja, Abeera A. Ansari, Syed S. Daood

**Acquisition, analysis, or interpretation of data:** Muhammad Rabah, Waqar Ul Habib Khan, Abeera A. Ansari, Syed S. Daood, Ali Raza

**Drafting of the manuscript:** Muhammad Rabah, Waqar Ul Habib Khan, Abeera A. Ansari, Syed S. Daood, Ali Raza

## Disclosures

**Human subjects:** All authors have confirmed that this study did not involve human participants or tissue. **Animal subjects:** All authors have confirmed that this study did not involve animal subjects or tissue. **Conflicts of interest:** In compliance with the ICMJE uniform disclosure form, all authors declare the following: **Payment/services info:** All authors have declared that no financial support was received from any organization for the submitted work. **Financial relationships:** All authors have declared that they have no financial relationships at present or within the previous three years with any organizations that might have an interest in the submitted work. **Other relationships:** All authors have declared that there are no other relationships or activities that could appear to have influenced the submitted work.

## Acknowledgements

The authors extend their appreciation to the Pakistan Science Foundation for their funding of PSF/CRP/C-NUST/T-Helix (47).

# References

1. Coal 2022 Analysis and forecast to 2025. (2022). Accessed: December 16, 2022: https://www.iea.org/reports/coal-2022.

2. Hossain N, Morni NAH: Co-pelletization of microalgae-sewage sludge blend with sub-bituminous coal as solid fuel feedstock. BioEnergy Research. 2020, 13:618-29.
3. Raza MA, Karim A, Aman M, Al-Khasawneh MA, Faheem M: Global progress towards the Coal: Tracking coal reserves, coal prices, electricity from coal, carbon emissions and coal phase-out. Gondwana Research. 2025, 139:43-72.
4. Isaac K, Bada SO: The co-combustion performance and reaction kinetics of refuse derived fuels with South African high ash coal. Heliyon. 2020, 6:03309.
5. Huang L, Liu J, He Y, et al.: Thermodynamics and kinetics parameters of co-combustion between sewage sludge and water hyacinth in CO2/O2 atmosphere as biomass to solid biofuel. Bioresource Technology. 2016, 218:631-42.
6. Gao N, Kamran K, Quan C, Williams PT: Thermochemical conversion of sewage sludge: A critical review. Progress in Energy and Combustion Science. 2020, 79:100843.
7. Aysu T, Durak H, Güner S, Bengü AŞ, Esim N: Bio-oil production via catalytic pyrolysis of Anchusa azurea: Effects of operating conditions on product yields and chromatographic characterization. Bioresource Technology. 2016, 205:7-14.
8. Banyhani ZM, Khan WUH, Abd El-Gawad HH, et al.: Synergistic transformation: Kinetic and thermodynamic evaluation of co-pyrolysis for low-rank bituminous coal and polyurethane foam waste. Process Safety and Environmental Protection. 2024, 184:907-21. 10.1016/j.psep.2024.01.041
9. Soria-Verdugo A, Goos E, Morato-Godino A, García-Hernando N, Riedel U: Pyrolysis of biofuels of the future: sewage sludge and microalgae-thermogravimetric analysis and modelling of the pyrolysis under different temperature conditions. Energy Conversion and Management. 2017, 138:261-72.
10. Mullen CA, Dorado C, Boateng AA: Catalytic co-pyrolysis of switchgrass and polyethylene over HZSM-5: Catalyst deactivation and coke formation. Journal of Analytical and Applied Pyrolysis. 2018, 129:195-203.
11. Lin L, Han X, Han B, Yang S: Emerging heterogeneous catalysts for biomass conversion: studies of the reaction mechanism. Chemical Society Reviews. 2021, 50:11270-1292. 10.1039/d1cs00039j
12. Shao J, Yan R, Chen H, Yang H, Lee DH: Catalytic effect of metal oxides on pyrolysis of sewage sludge. Fuel Processing Technology. 2010, 91:1113-118.
13. Zhao S, Wang DW, Amal R, Dai L: Carbon-based metal-free catalysts for key reactions involved in energy conversion and storage. Advanced Materials. 2019, 31:1801526.
14. Yuan X, Meng L, Zheng C, Zhao H: Deep insight into the mechanism of catalytic combustion of CO and CH4 over SrTi1-x B x O3 (B= Co, Fe, Mn, Ni, and Cu) perovskite via flame spray pyrolysis. ACS Applied Materials & Interfaces. 2021, 13:52571-2587.
15. Xu X, Zhong Y, Shao Z: Double perovskites in catalysis, electrocatalysis, and photo (electro) catalysis. Trends in Chemistry. 2019, 1:410-24. 10.1016/j.trechm.2019.05.006
16. Khan UM, Sarmad Q, Anwar M, et al.: Synthesis of cobalt loaded double perovskite SrTiFeO-δ (STF) as a stable catalyst for enhanced hydrogen production via methane decomposition. International Journal of Energy Research. 2021, 45:20073-20088. 10.1002/er.7084
17. Khan WUH, Khoja AH, Gohar WUH, et al.: In depth thermokinetic investigation on Co-pyrolysis of low-rank coal and algae consortium blends over CeO2 loaded hydrotalcite (MgNiAl) catalyst. Journal of Environmental Chemical Engineering. 2022, 10:108293. 10.1016/j.jece.2022.108293
18. Khan A, Saeed S, Pervaiz E, Khoja AH, Naqvi SR, Saeed S, Ali I: Comprehensive investigation of almond shells pyrolysis using advance predictive models. Renewable Energy. 2024, 227:120568. 10.1016/j.renene.2024.120568
19. Merdun H, Laougé ZB: Kinetic and thermodynamic analyses during co-pyrolysis of greenhouse wastes and coal by TGA. Renewable Energy. 2021, 163:453-64. 10.1016/j.renene.2020.08.120
20. Khoja AH, Gohar H, Khan WUH, et al.: Exploring copyrolysis characteristics and thermokinetics of peach stone and bituminous coal blends. Energy Science & Engineering. 2023, 11:4302-323. 10.1002/ese3.1583
21. Naqvi SR, Tariq R, Hameed Z, et al.: Pyrolysis of high ash sewage sludge: Kinetics and thermodynamic analysis using Coats-Redfern method. Renewable Energy. 2019, 131:854-60.
22. Tauseef M, Ansari AA, Khoja AH, Naqvi SR, Liaquat R, Nimmo W, Daood SS: Thermokinetics synergistic effects on co-pyrolysis of coal and rice husk blends for bioenergy production. Fuel. 2022, 318:123685. 10.1016/j.fuel.2022.123685
23. Yu J, Zeng X, Zhang J, Zhong M, Zhang G, Wang Y, Xu G: Isothermal differential characteristics of gas-solid reaction in micro-fluidized bed reactor. Fuel. 2013, 103:29-36.
24. Saeed S, Saleem M, Durrani A: Thermal performance analysis and synergistic effect on co-pyrolysis of coal and sugarcane bagasse blends pretreated by trihexyltetradecylphosphonium chloride. Fuel. 2020, 278:118240. 10.1016/j.fuel.2020.118240
25. Ashraf A, Sattar H, Munir S: Thermal decomposition study and pyrolysis kinetics of coal and agricultural residues under non-isothermal conditions. Fuel. 2019, 235:504-14. 10.1016/j.fuel.2018.07.120
26. Tariq R, Saeed S, Riaz M, Saeed S: Kinetic and thermodynamic evaluation of almond shells pyrolytic behavior using Coats-Redfern and pyrolysis product distribution model. Energy Sources, Part A: Recovery, Utilization, and Environmental Effects. 2023, 45:4446-462. 10.1080/15567036.2023.2202639
27. Munir S, Sattar H, Nadeem A, Azam M: Thermal and kinetic performance analysis of corncobs, Falsa sticks, and Chamalang coal under oxidizing and inert atmospheres. Energy Sources, Part A: Recovery, Utilization, and Environmental Effects. 2017, 39:775-82. 10.1080/15567036.2016.1263254
28. Saeed S, Shafeeq A, Raza W, Ijaz A, Saeed S: Effect of regenerated ionic liquid pretreatment on the thermogravimetric analysis of spent coffee ground. Energy Sources, Part A: Recovery, Utilization, and Environmental Effects. 2020, 1-13. 10.1080/15567036.2020.1773969
29. Dhar SA, Sakib TU, Hilary LN: Effects of pyrolysis temperature on production and physicochemical characterization of biochar derived from coconut fiber biomass through slow pyrolysis process. Biomass Conversion and Biorefinery. 2022, 12:2631-647.
30. Zhang C, Li S, Ouyang S, et al.: Co-pyrolysis characteristics of camellia oleifera shell and coal in a TGA and a fixed-bed reactor. Journal of Analytical and Applied Pyrolysis. 2021, 155:105035.
31. Cooke NE, Fuller OM, Gaikwad RP: FT-ir spectroscopic analysis of coals and coal extracts. Fuel. 1986, 65:1254-260.

32. Geng W, Nakajima T, Takanashi H, Ohki A: Analysis of carboxyl group in coal and coal aromaticity by Fourier transform infrared (FT-IR) spectrometry. Fuel. 2009, 88:139-44.
33. Yan J, Lei Z, Li Z, et al.: Molecular structure characterization of low-medium rank coals via XRD, solid state 13C NMR and FTIR spectroscopy. Fuel. 2020, 268:117038.
34. Sonibare OO, Haeger T, Foley SF: Structural characterization of Nigerian coals by X-ray diffraction, Raman and FTIR spectroscopy. Energy. 2010, 35:5347-353.
35. Song H, Liu G, Zhang J, Wu J: Pyrolysis characteristics and kinetics of low rank coals by TG-FTIR method. Fuel Processing Technology. 2017, 156:454-60.
36. Wang S, Tang Y, Schobert HH, Guo Y, Gao W, Lu X: FTIR and simultaneous TG/MS/FTIR study of Late Permian coals from Southern China. Journal of Analytical and Applied Pyrolysis. 2013, 100:75-80.
37. Thipkhunthod P, Meeyoo V, Rangsunvigit P, Rirksomboon T: Describing sewage sludge pyrolysis kinetics by a combination of biomass fractions decomposition. Journal of Analytical and Applied Pyrolysis. 2007, 79:78-85.
38. Sun H, Bi H, Jiang C, et al.: Experimental study of the co-pyrolysis of sewage sludge and wet waste via TG-FTIR-GC and artificial neural network model: Synergistic effect, pyrolysis kinetics and gas products. Renewable Energy. 2022, 184:1-14.
39. Liu R, Liu G, Yousaf B, Niu Z, Abbas Q: Novel investigation of pyrolysis mechanisms and kinetics for functional groups in biomass matrix. Renewable and Sustainable Energy Reviews. 2022, 153:111761.
40. Niu Z, Liu G, Yin H, Wu D, Zhou C: Investigation of mechanism and kinetics of non-isothermal low temperature pyrolysis of perhydrous bituminous coal by in-situ FTIR. Fuel. 2016, 172:1-10.
41. Wang Y, Jia L, Guo J, Wang B, Zhang L, Xiang J, Jin Y: Thermogravimetric analysis of co-combustion between municipal sewage sludge and coal slime: Combustion characteristics, interaction and kinetics. Thermochimica Acta. 2021, 706:179056.
42. Idris SS, Abd Rahman N, Ismail K, Alias AB, Abd Rashid Z, Aris MJ: Investigation on thermochemical behaviour of low rank Malaysian coal, oil palm biomass and their blends during pyrolysis via thermogravimetric analysis (TGA). Bioresource Technology. 2010, 101:4584-592.
43. Romanovskii V, Martsul V: Distribution of heteroatoms of synthetic ion exchangers in pyrolysis products. Russian Journal of Applied Chemistry. 2009, 82:836-39.
44. Naqvi SR, Tariq R, Hameed Z, et al.: Pyrolysis of high-ash sewage sludge: Thermo-kinetic study using TGA and artificial neural networks. Fuel. 2018, 233:529-38.
45. Ma J, Luo H, Li Y, Liu Z, Li D, Gai C, Jiao W: Pyrolysis kinetics and thermodynamic parameters of the hydrochars derived from co-hydrothermal carbonization of sawdust and sewage sludge using thermogravimetric analysis. Bioresource Technology. 2019, 282:133-41.
46. Merdun H, Laougé ZB, Çığgın AS: Synergistic effects on co-pyrolysis and co-combustion of sludge and coal investigated by thermogravimetric analysis. Journal of Thermal Analysis and Calorimetry. 2021, 146:2623-637.
47. Hameed Z, Aman Z, Naqvi SR, Tariq R, Ali I, Makki AA: Kinetic and thermodynamic analyses of sugar cane bagasse and sewage sludge co-pyrolysis process. Energy & Fuels. 2018, 32:9551-558. 10.1021/acs.energyfuels.8b01972
48. Folgueras MB, Díaz RM, Xiberta J: Pyrolysis of blends of different types of sewage sludge with one bituminous coal. Energy. 2005, 30:1079-91.
49. Guo F, Li X, Wang Y, Liu Y, Li T, Guo C: Characterization of Zhundong lignite and biomass co-pyrolysis in a thermogravimetric analyzer and a fixed bed reactor. Energy. 2017, 141:2154-163.
50. Naqvi SR, Uemura Y, Osman N, Yusup S: Kinetic study of the catalytic pyrolysis of paddy husk by use of thermogravimetric data and the Coats-Redfern model. Research on Chemical Intermediates. 2015, 41:9743-755.
51. Laura F, Tamara A, Müller A, Hiroshan H, Christina D, Serena C: Selecting sustainable sewage sludge reuse options through a systematic assessment framework: Methodology and case study in Latin America. Journal of Cleaner Production. 2020, 242:118389.
52. Ghetti P, Ricca L, Angelini L: Thermal analysis of biomass and corresponding pyrolysis products. Fuel. 1996, 75:565-73.
53. Meng A, Zhou H, Qin L, Zhang Y, Li Q: Quantitative and kinetic TG-FTIR investigation on three kinds of biomass pyrolysis. Journal of Analytical and Applied Pyrolysis. 2013, 104:28-37.
54. Chen X, Liu L, Zhang L, Zhao Y, Qiu P: Pyrolysis characteristics and kinetics of coal-biomass blends during co-pyrolysis. Energy & Fuels. 2019, 33:1267-278.
55. Ozbay N, Yargic AS, Sahin RZY, Yaman E: Valorization of banana peel waste via in-situ catalytic pyrolysis using Al-Modified SBA-15. Renewable Energy. 2019, 140:633-46.
56. Andrés ES, Toledano-Luque M, Prado A, et al.: Physical properties of high pressure reactively sputtered TiO2. Journal of Vacuum Science & Technology A. 2005, 23:1523-530.
57. Ahangaran F, Hassanzadeh A, Nouri S: Surface modification of Fe3O4@ SiO2 microsphere by silane coupling agent. International Nano Letters. 2013, 3:1-5.
58. Xie Q, Peng P, Liu S, et al.: Fast microwave-assisted catalytic pyrolysis of sewage sludge for bio-oil production. Bioresource Technology. 2014, 172:162-68.
59. Du S, Valla JA, Bollas GM: Characteristics and origin of char and coke from fast and slow, catalytic and thermal pyrolysis of biomass and relevant model compounds. Green Chemistry. 2013, 15:3214-229.
60. Sait HH, Hussain A, Salema AA, Ani FN: Pyrolysis and combustion kinetics of date palm biomass using thermogravimetric analysis. Bioresource Technology. 2012, 118:382-89.
61. Wang L, Lei H, Liu J, Bu Q: Thermal decomposition behavior and kinetics for pyrolysis and catalytic pyrolysis of Douglas fir. RSC Advances. 2018, 8:2196-202. 10.1039/c7ra12187c
62. Qu B, Zhang Y, Wang T, Li A, Wu Z, Ji G: Dynamic pyrolysis characteristics, kinetics and products analysis of waste tire catalytic pyrolysis with Ni/Fe-ZSM-5 catalysts using TG-IR-GC/MS. Catalysts. 2021, 11:1031.
63. Guo F, Li X, Liu Y, Peng K, Guo C, Rao Z: Catalytic cracking of biomass pyrolysis tar over char-supported catalysts. Energy Conversion and Management. 2018, 167:81-90.
64. Hu J, Danish M, Lou Z, Zhou P, Zhu N, Yuan H, Qian P: Effectiveness of wind turbine blades waste combined with the sewage sludge for enriched carbon preparation through the co-pyrolysis processes. Journal of Cleaner Production. 2018, 174:780-87.
65. Wahab MA, Ates F, Yildirir E, Miskolczi N: Investigation of thermal degradation kinetics and catalytic pyrolysis

of industrial sludge produced from textile and leather industrial wastewater. Biomass Conversion and Biorefinery. 2023, 13:11187-1201. 10.1007/s13399-021-02183-5
66. Zhang XY, Chen MQ: A comparison of isothermal with nonisothermal drying kinetics of municipal sewage sludge. Journal of Thermal Analysis and Calorimetry. 2016, 123:665-73.
67. Ma M, Xu D, Gong X, Diao Y, Feng P, Kapusta K: Municipal sewage sludge product recirculation catalytic pyrolysis mechanism from a kinetic perspective. Renewable Energy. 2023, 215:118955.
68. Yang J, Xu X, Liang S, et al.: Enhanced hydrogen production in catalytic pyrolysis of sewage sludge by red mud: thermogravimetric kinetic analysis and pyrolysis characteristics. International Journal of Hydrogen Energy. 2018, 43:7795-807.
69. Wang Y, Li Y, Wang G, et al.: Effect of Fe components in red mud on catalytic pyrolysis of low rank coal. Journal of the Energy Institute. 100:1-9.
70. Gohar H, Khoja AH, Ansari AA, et al.: Investigating the characterisation, kinetic mechanism, and thermodynamic behaviour of coal-biomass blends in co-pyrolysis process. Process Safety and Environmental Protection,. 2022, 163:645-58.
71. Hwang J, Rao RR, Giordano L, Katayama Y, Yu Y, Shao-Horn Y: Perovskites in catalysis and electrocatalysis. Science. 2017, 358:751-56. 10.1126/science.aam7092
72. Wang Y, Yang Z, Liu L: Perovskite-based catalysts for syngas upgrading by intensified steam reforming of biomass tar. ACS Sustainable Chemistry & Engineering. 2024, 12:15812-5837. 10.1021/acssuschemeng.4c04571
73. Xia S, Li K, Xiao H, et al.: Pyrolysis of Chinese chestnut shells: Effects of temperature and Fe presence on product composition. Bioresource Technology. 2019, 287:121444.
74. Ahmad I, Khan R, Ishaq M, Khan H, Ismail M, Gul K, Ahmad W: Valorization of spent lubricant engine oil via catalytic pyrolysis: Influence of barium-strontium ferrite on product distribution and composition. Journal of Analytical and Applied Pyrolysis. 2016, 122:131-41. 10.1016/j.jaap.2016.10.008
75. Yarbay Şahin RZ, Özbay N: Perspective on catalytic biomass pyrolysis bio-oils: essential role of synergistic effect of metal species co-substitution in perovskite type catalyst. Catalysis Letters. 2020, 151:1406-417. 10.1007/s10562-020-03394-7
76. Yang S, Zhang X, Chen L, et al.: Pyrolysis of sawdust with various Fe-based catalysts: Influence of support characteristics on hydrogen-rich gas production. Journal of Analytical and Applied Pyrolysis. 2019, 137:29-36.
77. Zhao X, Wang W, Liu H, Ma C, Song Z: Microwave pyrolysis of wheat straw: product distribution and generation mechanism. Bioresource Technology. 2014, 158:278-85.
78. Wu L, Liu Y, Zhang L, Zhao L: A green-chemical synthetic route to fabricate a lamellar-structured Co/Co (OH) 2 nanocomposite exhibiting a high removal ability for organic dye. Dalton Transactions. 2014, 43:5393-400.
79. Aysu T, Ola O, Maroto-Valer MM, Sanna A: Effects of titania based catalysts on in-situ pyrolysis of Pavlova microalgae. Fuel Processing Technology. 2017, 166:291-98.
80. Liu G, Song H, Wu J: Thermogravimetric study and kinetic analysis of dried industrial sludge pyrolysis. Waste Management. 2015, 41:128-33. 10.1016/j.wasman.2015.03.042
81. Mohamed BA, Li LY: Biofuel production by co-pyrolysis of sewage sludge and other materials: a review. Environmental Chemistry Letters. 2023, 21:153-82. 10.1007/s10311-022-01496-9